Published for SISSA by Springer

Received: April 15, 2026
Accepted: May 24, 2026
Published: July 3, 2026

# Multiplicity dependence of prompt and non-prompt J/$\psi$ production at midrapidity in pp collisions at $\sqrt{s} = 13$ TeV

## The ALICE collaboration

*Full author list at the end of the paper*

*E-mail:* ALICE-publications@cern.ch

Abstract: The yields of prompt and non-prompt J/$\psi$ and the fraction of non-prompt J/$\psi$ are measured at midrapidity ($|y| < 0.9$) via the dielectron decay channel as a function of the midrapidity charged-particle multiplicity ($|\eta| < 0.9$) in pp collisions at $\sqrt{s} = 13$ TeV. The J/$\psi$ yields and the multiplicity are normalized by their average value in inelastic collisions. The multiplicity-dependent yield ratio between prompt J/$\psi$ and $D^0$ is reported. The multiplicity is further divided into three azimuthal regions with respect to the J/$\psi$ momentum: toward the J/$\psi$ emission direction, transverse, or opposite to it. A stronger-than-linear increase of the self-normalized yields is observed for both prompt and non-prompt J/$\psi$ production, with similar trends. This behaviour is also observed in the toward region, while a weaker increase is observed in the transverse and away regions.

Keywords: Hadron-Hadron Scattering, Proton-Proton Scattering, Quarkonium

ArXiv ePrint: 2604.07968



https://doi.org/10.1007/JHEP07(2026)051

JHEP07(2026)051

## Contents



## 1 Introduction

Charmonia, such as J/$\psi$ mesons, are bound states of charm and anticharm quarks. They can be produced directly in the collision, arise from the decay of a higher charmonia state, or from the weak decays of open-beauty hadrons. In the first two cases, the charmonia are called prompt, and they are called non-prompt otherwise. While perturbative quantum chromodynamics (pQCD) calculations can describe the production cross section of a heavy-quark pair, its hadronization into a prompt J/$\psi$ meson cannot be computed from first principles and has to be described by phenomenological models. One of them is the Improved Color Evaporation Model (ICEM) [1], where the transition of a produced heavy-quark pair to a colorless state, by emitting soft gluons, happens with a fixed probability. Alternatively, in the Non-Relativistic QCD (NRQCD) model [2, 3], the heavy-quark pair may be produced in either a color-singlet or a color-octet state. The transition from these states to the physical quarkonium is described by Long-Distance Matrix Elements, which are extracted from global fits to data [4]. These calculations have also been complemented by taking into account the transverse momentum distribution of the initial gluons in the $k_{\mathrm{T}}$-factorization scheme [5, 6], or by calculating the gluon momentum distributions within the Color Glass

Condensate (CGC) framework [3]. In the latter, also contributions from triple gluon fusion have been included [7, 8].

The hadronization of the b quark to produce a non-prompt J/$\psi$ meson can be modelled by different mechanisms, such as fragmentation or coalescence. Recent measurements of baryon-to-meson ratios in the charm and beauty sectors in proton-proton (pp) collisions at $\sqrt{s} = 13$ TeV by ALICE [9, 10] and LHCb [11] show a non-universality of these hadronization mechanisms compared to $e^+e^-$ and ep collisions, as well as a dependence on the multiplicity [11–13].

Investigating the dependence of J/$\psi$ production on the charged-particle multiplicity (i.e. the number of charged particles produced in the collision) can provide valuable insights. Firstly, as most charged particles are produced in soft scatterings, the interplay between hard and soft particle production mechanisms can be investigated. Secondly, measurements of charged hadrons in high-multiplicity pp events at the LHC have shown signs of collectivity similar to those observed in the quark–gluon plasma (QGP) [14]. The strange particle yields are found to continuously increase as a function of the multiplicity from pp to p–Pb and Pb–Pb collisions [15–18]. This motivates further studies of high-multiplicity events, also for events containing heavy-flavoured particles. In addition, the comparison between the multiplicity dependence of prompt and of non-prompt J/$\psi$ production could help investigating the effects of the parton mass and of the hadronization mechanism on the measurements.

The multiplicity dependence of the self-normalized yields of J/$\psi$, $\psi(2S)$, and $\Upsilon(nS)$ mesons has been measured in pp collisions across various rapidity regions at the LHC by ALICE [19–24] and CMS [25], and at RHIC by PHENIX [26] and STAR [27, 28]. The yields are self-normalized, i.e. they are normalized by their average values in inelastic events. A stronger-than-linear increase of the yields with the self-normalized multiplicity is observed when the quarkonium and the multiplicity are measured in the same rapidity region and the J/$\psi$ decay daughters (two charged leptons) are included in the multiplicity calculation [20, 24, 28]. The increase is even stronger at higher quarkonium transverse momentum. However, when quarkonium and multiplicity are measured in different rapidity regions, the increase of the self-normalized yields with multiplicity is weaker. It is close to linear at LHC energies [21–23], and weaker than linear at RHIC energies [26]. A weaker-than-linear increase also occurs at RHIC energies when the quarkonium decay daughters are removed from the multiplicity calculation [26]. Several other measurements of hard particle production reported by ALICE, such as high-$p_{\mathrm{T}}$ hadrons [29], D-mesons [30] and electrons from heavy-flavour decays [31] in pp collisions at $\sqrt{s} = 5.02, 7$ and 13 TeV also show similar stronger-than-linear increases with multiplicity. In contrast, electrons from W boson decays in pp collisions at $\sqrt{s} = 13$ TeV show a near-linear increase [32].

The yield ratios of excited-to-ground quarkonium states have also been measured in pp collisions by ALICE [22, 23], LHCb [33, 34] and CMS [35] at the LHC, and by PHENIX [26] and STAR [28] at RHIC. ALICE, PHENIX and STAR results show a trend compatible with a flat behaviour, while the more precise measurements by LHCb and CMS of the prompt charmonium and bottomonium yield ratios indicate a decrease of these ratios as a function of multiplicity. CMS has also measured in pp collisions at $\sqrt{s} = 7$ TeV [35] the $\Upsilon(nS)$ ratios as a function of the multiplicity in the azimuthal direction towards, transverse, or opposite to the $\Upsilon$ emission direction. No major differences were found between these three cases. The decrease was also found to be stronger in isotropic events compared to jet-like events, for which no modification of the ratio with multiplicity is visible, suggesting that the decrease depends on underlying event properties.

The multiplicity dependence of $J/\psi$ and $\psi(2S)$ production was also measured in p–Pb collisions at $\sqrt{s_{NN}} = 5.02$ and 8.16 TeV by ALICE [23, 36, 37]. At midrapidity, the increase in the self-normalized $J/\psi$ yields as a function of the midrapidity multiplicity is also stronger than linear. The self-normalized $J/\psi$ yield increases more weakly at forward rapidity in the proton-going direction than at backward rapidity in the Pb-going direction. The probed Bjorken-$x$ values of the partons probed in the Pb nucleus are lower in the former case. For both forward and backward rapidities, the increase of $\psi(2S)$ yield has been found compatible with the one from $J/\psi$ within uncertainties.

Several theoretical models aim to describe the strong increase of the $J/\psi$ yield with multiplicity. The influence of the multiple partonic interactions (MPI) on the multiplicity dependence is considered in these models [38–51]. In addition, some models rely on initial-state effects inside the colliding protons, such as in the CGC framework. In this framework, the gluon density saturates due to non-linear effects at low $x$ [38, 39], and the three-Pomeron fusion can have a strong influence at high multiplicity [40, 41]. Other models rely on the Bjorken-$x$ dependent spatial distribution of gluons [42], or rely on parallels with the Glauber model in pA collisions [43, 44]. Other explanations include final-state effects, where the yield of soft particles could be additionally suppressed in high charged-particle density environments compared to low-density environments [45]. Event generators such as PYTHIA 8 [46, 47] or EPOS4 [48–51] typically implement several of the initial- and final-state effects in hard and soft MPI. These effects include, for example, reconnections between strings or hydrodynamic evolution in high charged-particle-density environments.

The ratio between prompt quarkonium and open charm production is a particularly appropriate discriminant because several experimental and theoretical uncertainties cancel out in the ratio. In Pb–Pb collisions, this ratio increases when going from semicentral to central collisions, as measured by ALICE at midrapidity at $\sqrt{s_{NN}} = 5.02$ TeV [16, 52], possibly due to regeneration of $J/\psi$ mesons from uncorrelated c and $\bar{c}$ quarks in a dense medium with a high number of $c\bar{c}$ pairs produced in the collision. In LHCb fixed-target Pb–Ne collisions $\sqrt{s_{NN}} = 68.5$ GeV, this ratio decreases with the system size [53]. The multiplicity dependence of the ratio in pp collisions could provide information on whether dense medium effects could also be seen in small systems.

The hardest scattering in a collision typically results in outgoing high-$p_T$ partons which fragment into jets, increasing the particle yield in a specific direction. In contrast, the region azimuthally transverse to that direction probes mostly the soft MPI in the event, giving a cleaner estimate of the underlying event activity [54–56]. Therefore, the separation of the multiplicity estimators in azimuthal regions can shed more light on the mechanisms causing the observed stronger-than-linear increase of the self-normalized $J/\psi$ yield [57]. Particles associated with the $J/\psi$ production can be found in a direction close to the one of the $J/\psi$ meson. These include, for example, the particles produced inside a jet cone, or in the same decay process of a common mother particle such as a beauty hadron or higher mass charmonium. The multiplicity azimuthally transverse to the J/$\psi$ emission direction mostly measures the underlying event activity. It might, however, contain initial-state or large-angle radiation produced in the same process as the one leading to the J/$\psi$ production. Finally, the opposite region can include the recoil of the process leading to the J/$\psi$ production. The correlation between the J/$\psi$ production and the event activity has also been studied in pp collisions via the J/$\psi$-hadron azimuthal correlations [58], measured by ALICE at $\sqrt{s} = 13\,\mathrm{TeV}$ and found in good agreement with PYTHIA, and the $p_{\mathrm{T}}$ fraction carried by the J/$\psi$ meson in jets, measured by LHCb [59] and ALICE [60] at $\sqrt{s} = 13\,\mathrm{TeV}$, and CMS at $\sqrt{s} = 5.02\,\mathrm{TeV}$ [61]. While some theoretical calculations can reproduce the latter measurement [62], the jet fragmentation to the J/$\psi$ meson is softer than predicted by PYTHIA.

This paper reports the measurement of prompt and non-prompt J/$\psi$ production as a function of multiplicity, in pp collisions at a center-of-mass energy of $\sqrt{s} = 13\,\mathrm{TeV}$. The data were collected with the ALICE detector during Run 2 of the LHC. The charged-particle multiplicity is measured in $|\eta| < 0.9$, both in full azimuthal angle and separated into three azimuthal regions relative to the J/$\psi$ emission direction. Section 2 describes the experiment and the data sample used. Section 3 explains the analysis procedure. Section 4 presents the results and discusses their interpretation. Finally, a summary and conclusions are given in section 5.

## 2 Experimental setup and data samples

The J/$\psi$ mesons are reconstructed in the dielectron decay channel using the central barrel of ALICE [63, 64]. The detectors used for the track reconstruction are the Inner Tracking System (ITS) [65] and the Time Projection Chamber (TPC) [66]. They both have a full azimuthal coverage and are placed within a magnetic field of 0.5 T in the beam direction. The ITS is the detector closest to the interaction point. Due to its high spatial resolution, it plays a main role in the reconstruction of both the primary collision vertex and the secondary vertices from long-lived weakly decaying particles. It consists of two layers of Silicon Pixel Detectors (SPD), located at radial distances of 3.9 and 7.6 cm from the interaction point, respectively, followed by two layers each of Silicon Drift Detectors (SDD) and Silicon Strip Detectors (SSD). The TPC is the main ALICE tracking detector and also performs particle identification using the specific energy loss in its gas volume. It provides accurate momentum resolution and particle separation over a broad momentum range around midrapidity.

The data samples used in this analysis have been recorded during the LHC Run 2 in pp collisions at a center-of-mass energy of $\sqrt{s} = 13\,\mathrm{TeV}$ using several event triggers. A Minimum-Bias (MB) trigger requires the simultaneous detection of a signal in the V0A ($2.8 < \eta < 5.1$) and V0C ($-3.7 < \eta < -1.7$), two scintillator arrays with fast readout which together form the V0 detector [67]. A High-Multiplicity (HM) trigger requires the sum of the signals in the V0A and V0C (denoted as V0M) to be higher than a threshold value. It selects the 0.1% of the collisions with the highest V0M signal. Therefore, the corresponding event class is called V0M 0–0.1%. Additionally, a trigger based on the Transition Radiation Detector (TRD) [68] is also used. The TRD is made of 522 chambers distributed in the full azimuth within $|\eta| < 0.84$. Each chamber contains a radiator, inducing transition radiation when ultra-relativistic electrons and positrons traverse it, as well as a drift chamber, where the energy deposition of the particles is measured. The TRD trigger is configured to select events containing at least one track with an online-computed $p_{\mathrm{T}}$ higher than 2 GeV/$c$ and with an energy deposition compatible with that of an electron. Additional selections on the event properties were applied in order to reject pileup events, as well as a selection on the longitudinal event vertex position of $|z| < 10$ cm to ensure uniform detector coverage. The selected data samples correspond to integrated luminosities of approximately 30 nb$^{-1}$, 1.8 pb$^{-1}$, and 8.8 pb$^{-1}$ for the MB, TRD, and HM triggers, respectively.

Several sets of Monte-Carlo (MC) simulations are used for the corrections applied in this analysis. The first simulates MB collisions and is used to correct the charged-particle multiplicity. Events are simulated using PYTHIA 8 [46] with Monash tune [69]. Particles are propagated through the ALICE detectors using GEANT3 [70]. Simulation of pileup events is also included. To account for the particle species-dependent detection efficiency, the relative abundances of pions, kaons, protons, and strange baryons in the simulation were reweighted to match those observed in the data. This reweighting follows the procedure described in ref. [71].

For the simulation of the prompt and non-prompt J/$\psi$ meson reconstruction, two MC samples are used. One has injected prompt J/$\psi$ mesons on top of PYTHIA 6.4 [72] inelastic events. In the other, the PYTHIA 6.4 events are required to contain a $\mathrm{b\bar{b}}$ quark pair. The b quarks are hadronized to B hadrons and then forced to decay via J/$\psi$ decay channels. The J/$\psi$ mesons are decayed via the dielectron channel using EvtGen [73], which implements the radiative QED corrections using PHOTOS [74]. The events are then propagated through the ALICE detectors using GEANT3 [70]. In addition, the track parameters and their covariance matrix are smeared in order to reproduce the secondary vertexing resolution observed in the data.

## 3 Analysis

The per-event yield of J/$\psi$ mesons is measured as a function of the charged-particle multiplicity. Both quantities are normalized by their average values in inelastic events containing at least one charged particle within $|\eta| < 1$ (an event class called INEL>0). The inclusive J/$\psi$ yield is separated into prompt and non-prompt components. The separation relies on the reconstruction of the secondary decay vertex. In the case of non-prompt J/$\psi$ mesons, it is displaced from the primary vertex by a distance on the order of hundreds of micrometers, due to the weak decay of the beauty hadron mother particles. The multiplicity is estimated in three regions with respect to the emission direction of the J/$\psi$ meson. The analysis is performed differentially in the J/$\psi$ transverse momentum ($p_{\mathrm{T}}$).

The multiplicity-dependent self-normalized yields are measured separately for two event classes, namely INEL>0 and V0M 0–0.1%. For the INEL>0 analysis, data from the MB-triggered and the TRD-triggered samples are used, and corrected for trigger efficiencies. The self-normalized yields obtained independently for both samples are combined together using, as a weight, the inverse of the quadratic sum of statistical and uncorrelated systematic uncertainties.



JHEP07(2026)051

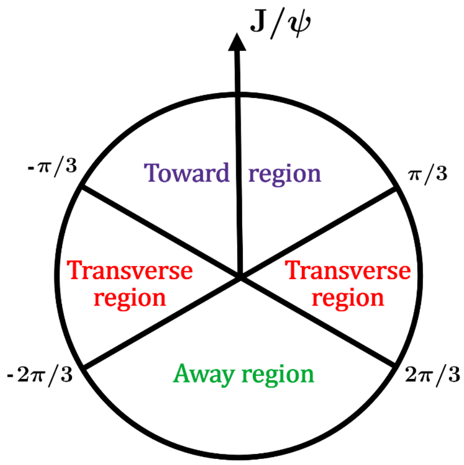


**Figure 1.** Regions in azimuthal angle defined with respect to a J/$\psi$ candidate.

### 3.1 Multiplicity estimator

The charged-particle multiplicity $N_{\mathrm{ch}}$ refers to the number of primary (i.e. with a proper lifetime larger than 1 cm/$c$ [75]) charged particles produced within $|\eta| < 0.9$. It is estimated based on the event multiplicity characterized by the number of global tracks, $N_{\mathrm{trks}}$, reconstructed both with the ITS and the TPC and with $p_{\mathrm{T}} > 0.15\,\mathrm{GeV}/c$. The track selection criteria are similar to those used in ref. [76].

In events containing a J/$\psi$ candidate, the multiplicity can be separated into several azimuthal regions relative to the J/$\psi$ emission direction. These azimuthal regions are as labelled in figure 1. The toward region contains all tracks with $|\varphi_{\mathrm{track}} - \varphi_{\mathbf{J}/\psi}| < \pi/3$. For the transverse region, the absolute azimuthal angle difference must be between $\pi/3$ and $2\pi/3$, while it must be larger than $2\pi/3$ for a track to be located in the away region.

In order to evaluate the multiplicity distribution of INEL>0 events in azimuthal regions, $N_{\mathrm{trks,region}}$, the tracks are counted in regions relative to an azimuthal angle selected randomly from a uniform distribution. Because the three regions span equal intervals in azimuth, their INEL>0 multiplicity distributions are identical.

### 3.2 Corrections to the multiplicity

Several corrections are applied to obtain the charged-particle multiplicity distribution from the event multiplicity. First, the event multiplicity distribution is corrected for the efficiency of the event selection criteria, i.e. the requirement of having a reconstructed vertex and the MB trigger selection. Both corrections affect mostly low-multiplicity events. The vertex reconstruction efficiency is estimated from data as a function of the event multiplicity. The MB trigger efficiency is estimated from MC simulations as a function of the V0 signal, and is further corrected to obtain an $N_{\mathrm{trks}}$-dependent efficiency using correlations between multiplicity estimators extracted from data.

An additional correction is applied to account for two effects: the inefficiency of detecting and reconstructing primary charged particles, and the remaining contamination from secondary or pileup particles. A detector response matrix, representing the correlations between the charged-particle multiplicity $N_{\rm ch}$ and the event multiplicity $N_{\rm trks}$, is extracted from the MB MC. An Iterative Bayesian Unfolding algorithm [77] uses this matrix and the $N_{\rm trks}$ distribution as an input in order to iteratively correct the full $N_{\rm ch}$ distribution. An unfolding matrix, which is an iterative correction of the detector response matrix, is also obtained at this stage.

In addition, the $N_{\rm trks}$ distribution is separated into several multiplicity intervals, in which the J/$\psi$ yields are also measured. The $N_{\rm ch}$ distribution corresponding to each of these intervals is then determined by convoluting the $N_{\rm trks}$ distribution in this interval with the unfolding matrix. The self-normalized multiplicity value corresponding to each $N_{\rm trks}$ interval is obtained by dividing the average value from this distribution by the multiplicity-integrated $\langle N_{\rm ch}\rangle_{\rm INEL>0}$ obtained in the MB sample. The same unfolding procedure is applied to correct the event multiplicity distribution in azimuthal regions.

### 3.3 J/$\psi$ selection

The J/$\psi$ candidates are built using all possible pairs of opposite-sign tracks, following a strategy which is similar to the one reported in refs. [20, 78]. The selected tracks are reconstructed in both the ITS and the TPC and are required to have $p_{\rm T} > 1$ GeV/$c$ and $|\eta| < 0.9$. A requirement of at least one hit in the SPD detector is imposed to ensure a good spatial resolution for secondary vertexing and to reject secondary electrons from photon conversions in the material outside of the SPD. In the TPC, the track candidates are required to have at least 70 clusters out of a maximum of 159 possible, which ensures good momentum and electron identification resolution. For electron identification, the specific energy loss (d$E$/d$x$) in the TPC is used. The signal is required to be within 3 standard deviations ($3\sigma$) with respect to the mean expected d$E$/d$x$ for electrons, as well as more than $3\sigma$ from the mean expected d$E$/d$x$ for both pions and protons. In the $p_{\rm T}$-differential analysis, the latter requirement on pion and proton rejection is loosened to $2.5\sigma$ for both tracks when the transverse momentum of the $\rm e^+e^-$ pair is larger than 8 GeV/$c$.

The invariant mass ($m_{ee}$) distribution of all pair candidates between 2 and 4 GeV/$c^2$ is extracted in each multiplicity interval. A binned likelihood fit of this distribution uses three templates, for combinatorial background, correlated background and signal. The combinatorial background is modelled using an event mixing technique, where events are grouped by longitudinal position of the vertex and event multiplicity. The normalization of the template is fixed such that the distribution of same-sign candidates from the mixed-event procedure matches the one from the same-event candidates. The correlated background is modelled by a second-order polynomial function. The shape of the signal is taken from the MC simulation with injected J/$\psi$ signals. The number of J/$\psi$ counts is obtained by subtracting the two background components and counting the remaining number of candidates in the mass range from 2.92 to 3.16 GeV/$c^2$.

### 3.4 Prompt and non-prompt J/$\psi$ separation

In order to separate prompt and non-prompt J/$\psi$ mesons, a Boosted Decision Tree (BDT) algorithm is used. The BDT is also used to reduce the background from uncorrelated $\rm e^+e^-$ pairs, which causes the signal-to-background ratio to decrease with $N_{\rm trks}$. The BDT is trained using the ROOT TMVA package [79]. Three classes are defined: background, prompt signal, and non-prompt signal. The sample of each class is further divided into independent training and testing samples. The background sample is taken from data, using $\mathrm{e^+e^-}$ pairs from the side-bands of the invariant mass distribution ($2 < m_{\mathrm{e^+e^-}} < 2.6\,\mathrm{GeV}/c^2$ and $3.2 < m_{\mathrm{e^+e^-}} < 4\,\mathrm{GeV}/c^2$). The prompt and non-prompt samples are taken from the dedicated MC simulation with injected $\mathrm{J}/\psi$ mesons. The training is done with seven variables. For each daughter, the deviation of $\mathrm{d}E/\mathrm{d}x$ from the mean electron hypothesis (in number of standard deviations), the distance of closest approach (DCA) in the transverse plane, and the hit map in the SPD are used. The last used variable is the pseudo-proper decay length of the pair, defined as

$$x = \vec{L} \cdot \frac{\vec{p_{\mathrm{T}}}}{p_{\mathrm{T}}} \frac{c\, m_{\mathbf{J}/\psi}}{p_{\mathrm{T}}}, \tag{3.1}$$

where $\vec{L}$ is the vector between the primary and secondary vertex, $p_{\mathrm{T}}$ is the transverse momentum of the $\mathrm{J}/\psi$ candidate, and $m_{\mathbf{J}/\psi}$ is the $\mathrm{J}/\psi$ mass [80]. The same BDT model is used for all multiplicity intervals.

The output of the BDT are probabilities for a candidate to belong to each of the three classes. In order to reduce the background, a selection is done by removing candidates with high BDT output probability to be background. The separation between prompt and non-prompt $\mathrm{J}/\psi$ mesons is done on a statistical basis, following a method described in detail in ref. [81]. The method is illustrated in figure 2. Using invariant mass fits, the number of raw inclusive $\mathrm{J}/\psi$ counts is extracted with different selections on the non-prompt BDT output probability. Each selection rejects candidates for which this output is lower than a chosen value, modifying the fraction of prompt and non-prompt components. The number of prompt and non-prompt $\mathrm{J}/\psi$ counts in the original sample is then extracted from a two-components fit. This fit uses as templates the BDT selection-dependent efficiencies estimated from the BDT testing sample. It consists in minimizing a $\chi^2$ which also takes into account the correlations between the number of raw counts with different selections,

This method has been compared to another method using a two-dimensional likelihood fit on the dielectron invariant mass and pseudo-proper decay length, described in detail in refs. [82, 83]. Both results agree within uncertainties.

### 3.5 Corrections to the J/$\psi$ yields and non-prompt fraction

**Self-normalized J/$\psi$ yields.** The self-normalized yields in the $N_{\mathrm{trks}}$ interval $i$ in each of the three triggered samples are defined as

$$(N_{\mathbf{J}/\psi}/\langle N_{\mathbf{J}/\psi}\rangle_{\mathrm{INEL}>0})_i = \frac{N^i_{\mathbf{J}/\psi,\,\mathrm{raw}}/(A^i \times \varepsilon^i)}{N^i_{\mathrm{evt,\,corr}}} \frac{N^{\mathrm{INEL}>0}_{\mathrm{evt,\,corr}}}{N^{\mathrm{INEL}>0}_{\mathbf{J}/\psi,\,\mathrm{raw}}/(A^{\mathrm{INEL}>0} \times \varepsilon^{\mathrm{INEL}>0})}. \tag{3.2}$$

Here, $A$ and $\varepsilon$ are the acceptance and reconstruction efficiency (including track and pair mass selections) estimated from MC, either in the specific $N_{\mathrm{trks}}$ interval (for $A^i$ and $\varepsilon^i$) or using the entire INEL>0 event sample (for $A^{\mathrm{INEL}>0}$ and $\varepsilon^{\mathrm{INEL}>0}$). $N^i_{\mathbf{J}/\psi,\,\mathrm{raw}}$ and $N^{\mathrm{INEL}>0}_{\mathbf{J}/\psi,\,\mathrm{raw}}$ are the number of raw prompt or non-prompt $\mathrm{J}/\psi$ counts in the $i$th $N_{\mathrm{trks}}$ interval and the INEL>0 sample, respectively. The $\mathrm{J}/\psi$ counts are estimated from the BDT cut

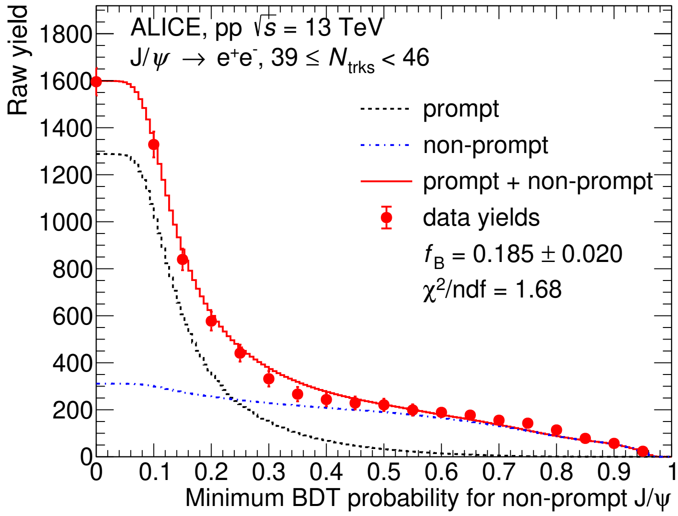


**Figure 2.** Raw inclusive J/$\psi$ yield as a function of the selection on the BDT non-prompt output probability for $39 \leq N_{\mathrm{trks}} < 46$, and $p_{\mathrm{T}} > 1\,\mathrm{GeV}/c$. The error bars indicate statistical uncertainties. The lines correspond to the prompt (dashed), non-prompt (dot-dashed) and total (continuous) J/$\psi$ scaled efficiencies. See text for more details.

variation method. In addition, for TRD-triggered data, a correction is done for the J/$\psi$ trigger efficiency, described later in this section.

$N^{i}_{\mathrm{evt,\,corr}}$ is the number of events in the specific $N_{\mathrm{trks}}$ interval, while $N^{\mathrm{INEL>0}}_{\mathrm{evt,\,corr}}$ is the total number of events in the MB-triggered sample. Both quantities are corrected for vertex reconstruction efficiency, and for MB trigger efficiency in the INEL>0 event class.

In eq. (3.2), $N^{i}_{\mathbf{J}/\psi,\,\mathrm{raw}}$ and $N^{i}_{\mathrm{evt,\,corr}}$ are estimated in the respective samples (MB, HM, TRD), while the INEL>0 quantities are estimated from the MB sample. The exception is in the TRD-triggered case, for which $N^{\mathrm{INEL>0}}_{\mathbf{J}/\psi,\,\mathrm{raw}}$ is also estimated from the TRD-triggered sample and the number of events, both in $N_{\mathrm{trks}}$ intervals and INEL>0, is estimated from the MB-triggered sample.

**Non-prompt fraction.** The non-prompt fraction $f_{\mathrm{B}}$ in a given $N_{\mathrm{trks}}$ interval is estimated as the ratio between the non-prompt J/$\psi$ yield and the sum of prompt and non-prompt yields in the same interval. All yields have been corrected for acceptance and efficiency following eq. (3.2).

**Corrections to the MC.** A number of corrections are applied to this MC sample in order to improve the description of data and obtain a correct efficiency in the different multiplicity intervals. The worse vertex resolution at lower multiplicity impacts the efficiency of the BDT. The multiplicity distributions of MC signals are therefore corrected with multiplicity-dependent weights. These weights are taken from a parametrization of the multiplicity-dependent J/$\psi$ yield and of the non-prompt fraction obtained after the first iteration of the algorithm. The $p_{\mathrm{T}}$ distributions also vary with multiplicity. Following a method similar to the one described in ref. [36], the $N_{\mathrm{trks}}$ dependence of $\langle p_{\mathrm{T}} \rangle$ of inclusive J/$\psi$ mesons is determined. The $\langle p_{\mathrm{T}} \rangle$ increases with multiplicity. A $p_{\mathrm{T}}$-dependent weight is applied in every multiplicity interval in order to reproduce the hardening of the spectrum. Finally, since the $p_T$ dependence of the ratios between different beauty hadrons is not reproduced in PYTHIA 8 by the Monash tune, for non-prompt $J/\psi$ mesons, the beauty hadron fractions in the PYTHIA 8 sample are reweighted to reproduce the Color Reconnection (CR) model Beyond Leading Color (CR-BLC) mode 2 [47] process.

**Additional corrections to the $J/\psi$ yields.** Due to the selections, the decay daughters of a reconstructed $J/\psi$ candidate are more likely to be included in the multiplicity estimator than typical primary particles. This effect artificially enhances the measured multiplicity in events containing a $J/\psi$ candidate. In order to remove this effect, when computing the event multiplicity for a given $J/\psi$ candidate, each $J/\psi$ decay daughter is counted with a probability exactly equal to the average track-level efficiency. This is done regardless of the track selection criteria the daughter may pass.

In addition, a bin-migration effect appears because a selected interval (bin) in $N_{\text{trks}}$ contains a large variation in $N_{\text{ch}}$ values, with different $J/\psi$ production yields. A correction of the measured $J/\psi$ yields is applied so that they correspond to the yields which would be obtained with only events having the exact value of self-normalized multiplicity considered. This reduces the dependence on the choice of the $N_{\text{trks}}$ intervals. This correction, typically of a few percent, depends on the variance of the $N_{\text{ch}}$ distribution within an $N_{\text{trks}}$ interval and on the second-order derivative of the self-normalized $J/\psi$-$N_{\text{ch}}$ correlation. The latter is estimated from a power-law fit. A toy model was used to validate these corrections.

For TRD-triggered data, the trigger efficiency is assumed to be the combination of two components: the self-trigger efficiency and the Underlying Event (UE) trigger efficiency. The self-trigger efficiency $\varepsilon(p_{\text{T}_{J/\psi}})$ represents the efficiency for the event to be triggered by one of the $J/\psi$ decay daughters. It is estimated from a data-driven method similar to the one described in ref. [84], where the single electron efficiency, obtained by analyzing events in the MB sample which also pass the TRD trigger requirements, is combined to a pair efficiency using $J/\psi$ decay kinematics. The underlying event trigger efficiency $\varepsilon_{\text{UE}}(N_{\text{trks}})$ represents the probability for the event in which the $J/\psi$ meson is produced to be triggered by another particle than the $J/\psi$ meson. It is determined from data as a function of event multiplicity. It also contains the small probability to be triggered by a correlated electron from the decay of the other B hadron in the non-prompt case, estimated from PYTHIA 8 simulations. The TRD trigger efficiency $\varepsilon_{\text{TRD}}$ can therefore be written as

$$\varepsilon_{\text{TRD}} = \varepsilon(p_{\text{T}_{J/\psi}}) + \varepsilon_{\text{UE}}(N_{\text{trks}}) - \varepsilon(p_{\text{T}_{J/\psi}}) \times \varepsilon_{\text{UE}}(N_{\text{trks}})\,, \tag{3.3}$$

where the product corrects for double-counting. The measurement is corrected for this efficiency during signal extraction by applying a weight to each $J/\psi$ candidate equal to $1/\varepsilon_{\text{TRD}}$.

### 3.6 Systematic uncertainties

**Self-normalized multiplicity.** For the self-normalized multiplicity, the systematic uncertainties which are considered are: the trigger efficiency, the unfolding procedure, the MC generator, and the data-MC discrepancy in tracking. All the uncertainties are added in quadrature.

| Source | $N_{\rm ch}/\langle N_{\rm ch}\rangle_{\rm INEL>0}$ | $N_{\rm ch,region}/\langle N_{\rm ch,region}\rangle_{\rm INEL>0}$ |
|---|---|---|
| MB trigger efficiency | 1.3% | 1.3% |
| Unfolding | 0.0 – 0.2% | 0.0 – 0.3% |
| MC generator | 0.0 – 2.0% | 0.4 – 4.0% |
| Tracking efficiency | 0.1 – 0.3% | 0.1 – 0.2% |
| Total | 1.3 – 2.4% | 1.4 – 4.2% |

**Table 1.** Summary of the systematic uncertainty contributions for the estimation of the self-normalized multiplicity azimuthally-integrated and in azimuthal regions.

The trigger efficiency uncertainty was reported to be 1.3% for INEL>0 events [20], and affects all intervals through the self-normalization. This value was estimated by comparing the trigger efficiency obtained from MC with an estimation which is done using data triggered by a logical OR between the V0A and the V0C.

To estimate the systematic uncertainty of the unfolding, the number of iterations is varied, and the results are compared to the ones obtained with a different unfolding algorithm (Iterative Dynamically Stabilized [85]). No significant differences are observed. A MC closure test further confirms the robustness of the unfolding procedure. In addition, the $N_{\rm ch}$ distribution after unfolding is folded again using the detector response matrix. The self-normalized $N_{\rm trks}$ values obtained are similar to the ones before unfolding at the per mille level. The impact of the MC statistics is checked by extrapolating the detector response matrix at high multiplicity. A difference of only 0.2% is observed for the highest multiplicity, negligible otherwise.

For the uncertainty due to the event generators, the results with detector response matrices obtained using PYTHIA 8 and EPOS LHC simulations are compared. This probes differences in the particle composition and $p_{\rm T}$ distribution of charged particles, as well as uncertainties due to the correction procedure of the particle composition in MC. The uncertainty reaches a maximum of 2% (4% for azimuthal regions) in the lowest multiplicity bin.

To evaluate the systematic uncertainty related to tracking, the analysis of the multiplicity distribution is repeated using track quality criterion variation. The difference in $\langle N_{\rm ch}\rangle$ with different selections, as well as ITS-TPC matching uncertainties, is used in order to estimate a tracking uncertainty for global tracks. This tracking uncertainty is applied by modifying the track reconstruction probability in MC. The analysis is repeated with this modified detector response matrix. The difference from standard results is found to be at most 0.3%.

A summary of the systematic uncertainties is shown in table 1.

**Non-prompt fraction and self-normalized J/$\psi$ yields.** For the non-prompt fraction and self-normalized yields, the systematic uncertainties which are considered are: the trigger efficiency, the unfolding procedure, the signal extraction, the BDT training, the BDT selection cuts, the simulated $p_{\rm T}$ spectrum of J/$\psi$ production, the beauty hadron compositions, the primary vertex calculation, as well as the possibly modified tracking efficiency in events with a J/$\psi$ meson compared to unbiased events. Unless stated otherwise, all uncertainties are calculated by evaluating the non-prompt fraction as well as the self-normalized prompt and non-prompt J/$\psi$ yields for each of the variations, and taking the RMS.



JHEP07(2026)051

The efficiency of the MB trigger can affect the J/$\psi$ yields through both the number of inelastic events and the number of J/$\psi$ counts. For the former case, an uncertainty due to this effect was already assigned to the self-normalized multiplicity. Because the trend followed by the data is little affected by variations of this efficiency, no additional uncertainty is assigned for the yields. For the latter case, some J/$\psi$ mesons might escape the trigger selection. Their number was estimated through the MB MC simulations. It was found to be below 2% in the lowest multiplicity interval, and below 0.2% otherwise. For the TRD trigger efficiency, the uncertainty of the self-trigger efficiency mostly cancels in the self-normalization. The UE efficiency has also been varied by $\pm 15\%$, which is the discrepancy between estimated and true UE efficiency observed in an independent PYTHIA 8 standalone simulation.

The uncertainty related to the correction for bin migration is evaluated by comparing the correction obtained when using a power-law fit and the one using a second-order polynomial fit, both with a null value at the origin and with a small offset.

The uncertainty due to signal extraction is estimated by changing the fit range, the signal mass window, and the background shape. For the latter, the combinatorial background is changed from mixed-event to like-sign estimation, and the correlated background shape is varied from a second-order polynomial to an exponential.

For the BDT training uncertainty, the analysis is repeated with different training parameters. The separation between the training and testing samples is also randomly modified twenty times. Modification of the BDT selections provides a check on the reproduction in the MC of the variables used for the BDT, as well as on the instabilities in the $\chi^2$ minimization procedure. The rejection value on the BDT background output probability is modified, as well as the number and values of selections in the BDT non-prompt output probability.

A systematic uncertainty might arise from possible differences between the real and simulated J/$\psi$ $p_{\mathrm{T}}$ spectra. To estimate the impact of these differences, different $p_{\mathrm{T}}$ distributions are used for calculating the acceptance, reconstruction efficiency, and BDT selection efficiency. The default prompt $p_{\mathrm{T}}$ shape in MB events is based on a fit to prompt cross section data at $\sqrt{s} = 13\,\mathrm{TeV}$ [83], while its variation is taken from PYTHIA 8 with the Monash tune [69]. The default non-prompt $p_{\mathrm{T}}$ shape in MB events is taken from PYTHIA 8 with Monash tune, while its variation is obtained from a Fixed Order plus Next-to-Leading Logarithm (FONLL) [86, 87] calculation. The evolution of $\langle p_{\mathrm{T}} \rangle$ with multiplicity is, as a variation, taken from PYTHIA 8 (Monash tune with oniaShower settings [88]) for prompt and non-prompt J/$\psi$ production independently. The beauty hadron fractions, assumed by default to be independent on the multiplicity, are also varied using the multiplicity dependence observed in PYTHIA 8 with CR-BLC mode 2.

An uncertainty for the description of the primary vertex is evaluated by removing the J/$\psi$ candidate decay daughters from the primary vertex calculation, and computing the difference to the default variation, affecting mainly the lowest multiplicities.

Finally, the reconstruction efficiency for tracks in the multiplicity estimator could be different in events containing a J/$\psi$ meson compared to MB events. For the non-prompt J/$\psi$ yields, the effect of a few additional non-prompt tracks with lower selection efficiency was studied using a toy model. This toy model was also used to estimate the error coming from the method for counting the J/$\psi$ decay daughters, when assuming that there is a mismatch

| Source | Prompt J/$\psi$ | | Non-prompt J/$\psi$ | | $f_B$ | |
|---|---|---|---|---|---|---|
| | (1) | (2) | (1) | (2) | (1) | (2) |
| MB trigger | 0.2% | 0.2% | 0.1% | 0.1% | 0.0% | 0.0% |
| Bin migration | 1.1% | 0.7% | 0.9% | 0.6% | 0.3% | 0.1% |
| Signal extraction | 0.7% | 2.9% | 2.2% | 2.1% | 2.8% | 4.5% |
| BDT training | 0.3% | 1.6% | 1.7% | 5.1% | 1.4% | 2.6% |
| BDT selections | 0.5% | 1.4% | 1.6% | 5.5% | 2.6% | 3.0% |
| $p_T$ distribution | 1.6% | 0.3% | 0.5% | 0.5% | 2.3% | 1.9% |
| B hadrons composition | 0.0% | 0.1% | 0.2% | 0.7% | 0.2% | 0.7% |
| Vertex reconstruction | 0.2% | 0.3% | 0.8% | 0.0% | 0.6% | 0.0% |
| TRD trigger efficiency | 0.1% | – | 0.0% | – | 0.3% | – |
| Tracking eff. in J/$\psi$ events | 0.3% | 0.0% | 1.3% | 1.0% | 1.6% | 1.3% |
| Total | 2.2% | 3.8% | 4.5% | 8.0% | 5.1% | 5.9% |

**Table 2.** Example of systematic uncertainty contributions for the prompt and non-prompt self-normalized J/$\psi$ yields, and for the non-prompt fraction $f_B$. The uncertainties are shown for $p_T > 1$ GeV/$c$, in the interval $15 \leq N_{trks} \leq 19$ for INEL>0 sample (noted as (1)), and in the interval $39 \leq N_{trks} \leq 45$ for HM sample (noted as (2)).

of 3% between the true tracking efficiency and the one used in the reconstruction. For the measurement in azimuthal regions, the track reconstruction, J/$\psi$ selection, and TRD trigger efficiency depend slightly on the azimuthal angle. The variation of the efficiency in each of the three regions of $|\varphi_{track} - \varphi_{J/\psi}|$ compared to MB events does not exceed 0.3%. This was also converted to an uncertainty on the multiplicity-dependent J/$\psi$ yields using a toy model.

The systematic uncertainties from all the sources described here are assumed to be uncorrelated and added in quadrature. A typical example of the systematic contributions for prompt and non-prompt self-normalized yields, as well as for $f_B$, for two intervals of $N_{trks}$, is shown in table 2.

## 4 Results and discussion

### 4.1 Multiplicity-dependent prompt and non-prompt J/$\psi$ yields

The fraction of J/$\psi$ mesons with $p_T > 1$ GeV/$c$ coming from the decay of beauty hadrons, $f_B$, is shown in figure 3 as a function of self-normalized multiplicity, for both the INEL>0 (full markers) and V0M 0–0.1% (open symbols) data samples. For all the measurements presented in this section, the decay products of the J/$\psi$ meson are kept in the multiplicity count. A more thorough discussion on this choice can be found in appendix A. This fraction provides insight into the difference between charm and beauty production mechanisms. In the lowest multiplicity interval, $f_B$ has a relatively small value compared to higher event multiplicities. This is expected due to the larger associated multiplicity expected in beauty-hadron decays compared to prompt J/$\psi$ decays. For higher multiplicities, a linear fit, excluding the first multiplicity interval, deviates from a flat trend by 2.9$\sigma$, suggesting a hint of an increase with multiplicity.

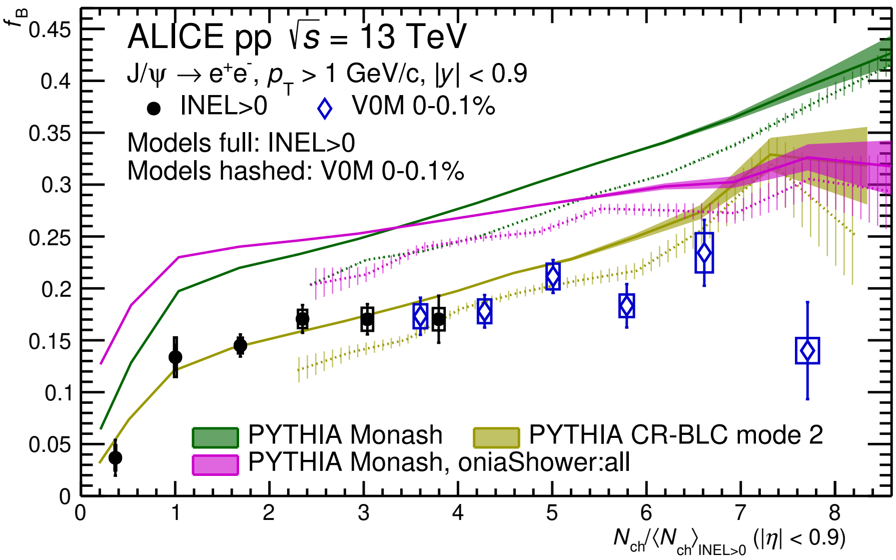


**Figure 3.** Fraction of non-prompt J/$\psi$ mesons, $f_B$, for $p_T > 1$ GeV/$c$ as a function of the self-normalized charged-particle multiplicity measured within $|\eta| < 0.9$ for the INEL>0 (full markers) and V0M 0–0.1% (open markers) event classes. The vertical bars and boxes indicate the statistical and systematic uncertainties, respectively. The results are compared to PYTHIA 8 simulations using different tunes, as indicated by the legend [46, 47, 88]. The PYTHIA calculations emulating the V0M 0–0.1% class (0.1% highest multiplicity events in the V0 acceptance) are shown as hashed lines.

The data are compared to PYTHIA 8.311 simulations using several different settings: the Monash tune [69], the CR-BLC mode 2 process [47], and the oniaShower process [88] with the Monash tune. PYTHIA is a MC generator which simulates sequentially multiple partonic interactions. These can further be evolved through partonic showers. Hadronization occurs via the breaking of strings between quarks and gluons. The CR mechanism allows the strings to be reorganized in order to minimize the string length. CR is improved with the CR-BLC mechanisms, which, by rearranging the color flow in the event, could strongly impact the multiplicity. Prompt quarkonia are produced by using the NRQCD framework [89–91], typically in the initial hard scattering. When the oniaShower process is activated, quarkonia are produced within partonic showers, using splitting kernels for the emission of heavy quark-antiquark pairs.

The data in the next figures are also compared to EPOS4HQ1.0 [48–51], an event generator implementing parallel scatterings between projectile and target nucleons. A dynamical saturation scale, dependent on the momentum fraction but also on the number of such scatterings, is introduced in the calculation in order to ensure that the factorization theorem holds and to model non-linear effects. The partonic ladders from the scatterings are further evolved in a core-corona procedure. The high energy-density core evolves hydrodynamically while the lower energy-density corona directly enters hadronization. The evolution of the core can also be deactivated. Heavy quarks are created in the partonic ladder and interact in the medium via elastic and radiative collisions, then hadronize via coalescence or fragmentation [92, 93]. If a charm and an anticharm quark are close in position space and momentum, they can also hadronize together by coalescence to form a quarkonium. The quarks are assumed to be initially closer in position space when they come from the same heavy-quark pair [94]. The fill areas for the PYTHIA and EPOS4 curves represent statistical uncertainties. They are sizeable at high multiplicity especially for EPOS4 with hydrodynamic evolution.

The prompt $J/\psi$ results are further compared to two CGC-based calculations. The first one, uses the CGC initial-state condition together with the Improved Color Evaporation Model (CGC+ICEM) [38]. High-multiplicity events are modelled with a higher saturation scale, modifying the gluon distribution inside the proton. A second calculation employs the 3-Pomeron Color Glass Condensate model (3-Pomeron CGC) [40, 41]. The 3-Pomeron fusion mechanism enhances the associated multiplicity compared to 2-Pomeron fusion, by increasing the possible fluctuations in the multiplicity produced by each Pomeron.

The self-normalized multiplicity distributions are well reproduced by the models, with a discrepancy of no more than 20% until at least 5 times the average multiplicity, and a larger discrepancy for higher multiplicities. In order to compare the model calculations to the ALICE HM-triggered data, a similar selection as for the data is performed, namely for the 0.1% events with the highest charged-particle multiplicity in the acceptance of the V0 detector. The model calculations with these selections are shown as hashed curves in the figures. An inspection on the MC revealed a small impact of the V0 detector effects on the correlation compared to the data uncertainties, due to the requirement in the models not being applied on the V0M signal but on the multiplicity in the V0 acceptance. According to the MC simulations based on these models, the HM trigger selection induces a bias on the measured $f_{\mathrm{B}}$ at a given event multiplicity compared to the same observable in INEL>0 events. Such a bias has also been observed when analyzing jet production [95]. In a naive scenario in which the high multiplicity requirement at forward rapidity implicitly selects events with enhanced beauty-quark pair production at forward rapidity, a reduction of $f_{\mathrm{B}}$ at midrapidity is expected. Overall, the model calculations overestimate the non-prompt fraction, with the exception of the CR-BLC PYTHIA settings.

In the upper panels of figure 4, the self-normalized yields of prompt and non-prompt $J/\psi$ mesons are shown as a function of the charged-particle multiplicity. Both the $J/\psi$ yields and the multiplicity are normalized by their average value in INEL>0 events, see eq. (3.2). A dashed grey line representing a linear increase with slope 1 ($y = x$) is also drawn for reference and illustration purposes. The bottom panels show the ratio between the data points and the linear reference. Both prompt and non-prompt $J/\psi$ yields show a stronger-than-linear increase with multiplicity, similar to the one found for inclusive $J/\psi$ yield [20]. The increase of $J/\psi$ yield with multiplicity is similar for the prompt and non-prompt components, as expected from the mild dependence of the $f_{\mathrm{B}}$ with multiplicity.

The stronger-than-linear increase could be interpreted as a larger saturation for soft particle production than for hard particle production in high-density environments, or as an increase in the associated particle production for hard probes. Comparisons of the measurements to PYTHIA calculations show that the Monash tune underestimates the prompt $J/\psi$ yield for multiplicities higher than four times the average multiplicity. The CR-BLC mode 2 settings, shown separately in appendix B for visibility, present a similar increase to the Monash tune. In contrast, the oniaShower option is in very good agreement with the



JHEP07(2026)051

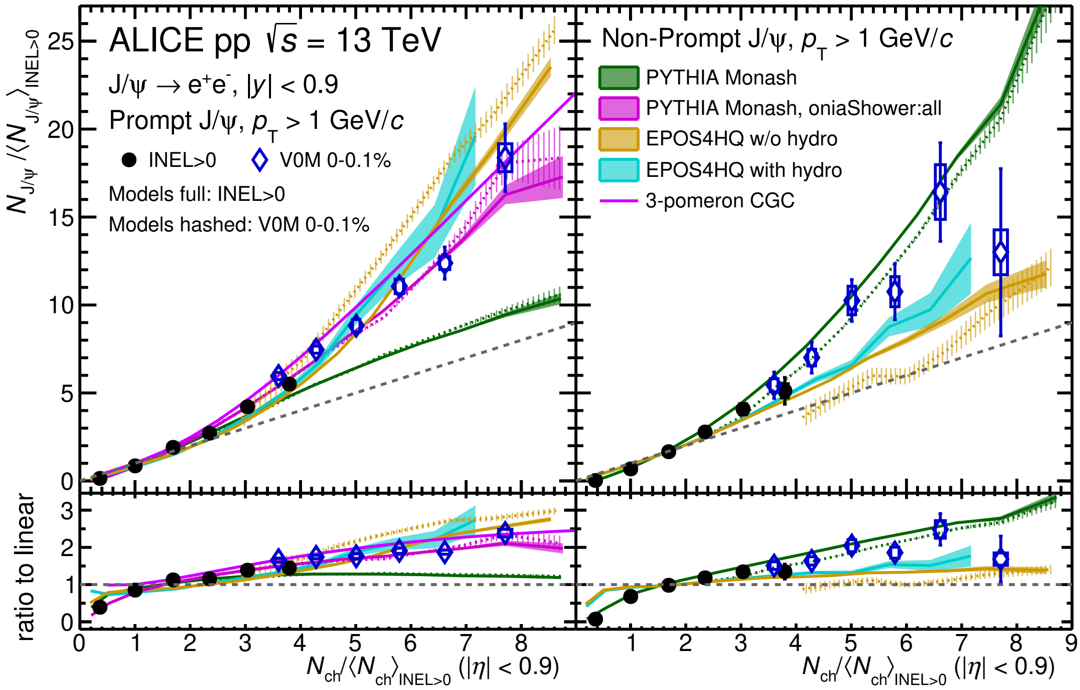


**Figure 4.** Self-normalized prompt (left) and non-prompt (right) J/$\psi$ yields with $p_{\rm T} > 1$ GeV/$c$ as a function of self-normalized charged-particle multiplicity at midrapidity. The data are shown separately for the INEL>0 and V0M 0–0.1% event classes. The yields are compared to PYTHIA 8 using different settings [69, 88], as well as EPOS4 [48–51] and the 3-Pomeron CGC model [40, 41]. Lower panels show the ratios to the expectation from a linear increase. The vertical bars and boxes indicate the statistical and systematic uncertainties, respectively.

data. This could indicate that, due to the additional particles emitted in the parton shower, the production process of the J/$\psi$ meson has a strong influence on the multiplicity-dependent J/$\psi$ yield, and that higher-order corrections are important to describe quarkonium production. For non-prompt J/$\psi$ production, the Monash tune reproduces the trend as a function of multiplicity well. The oniaShower process is not shown since it only affects prompt J/$\psi$ production. As was also seen for $f_{\rm B}$, PYTHIA calculations predict that, at a given multiplicity, the self-normalized yield obtained for non-prompt J/$\psi$ production is lower in HM-triggered events than in INEL>0 events. The prompt J/$\psi$ production seems less affected by this trigger bias, as estimated from PYTHIA. The 3-Pomeron CGC calculation shows a good agreement to the prompt J/$\psi$ data over the entire multiplicity range. The EPOS4 calculations, with and without the hydrodynamic evolution, describe the prompt J/$\psi$ measurements fairly well, except for a tendency to slightly overshoot the V0M 0–0.1% results. The strong increase in this case is mainly due to the combinatorial enhancement from c and $\bar{\rm c}$ coming from different c$\bar{\rm c}$ pairs, more frequent at higher multiplicities [94]. A slightly stronger increase is found with hydrodynamic evolution compared to without, due to a reduction in the multiplicity for which the available energy has been transferred to radial flow [48]. EPOS4 calculations underestimate the non-prompt J/$\psi$ measurements for a self-normalized multiplicity above 3.



JHEP07(2026)051

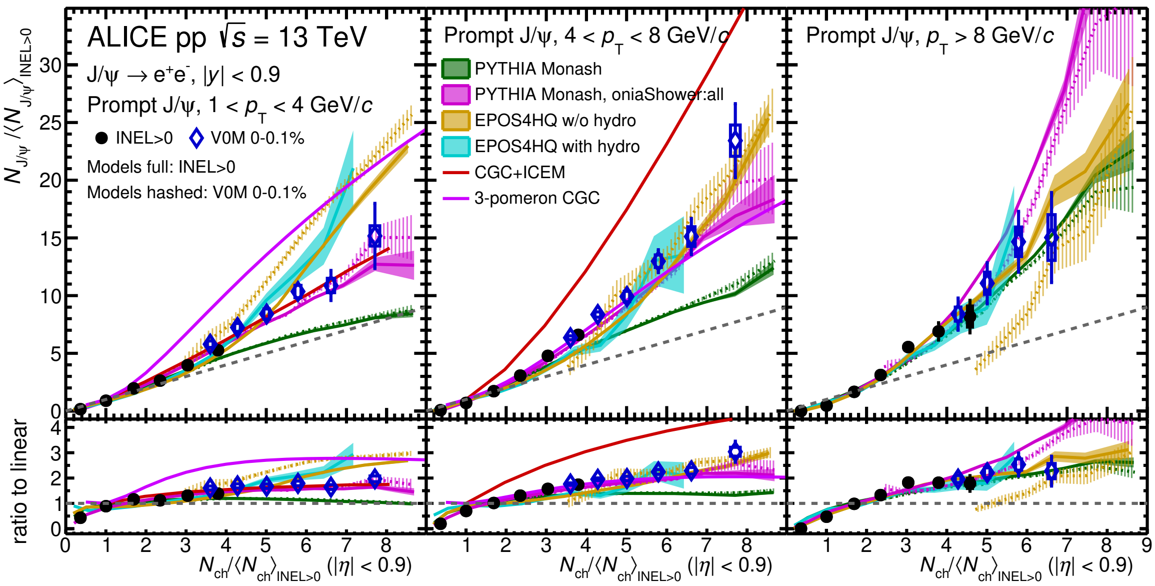


**Figure 5.** Prompt $J/\psi$ yield for $1 < p_{\mathrm{T}} < 4$ GeV/$c$ (left), $4 < p_{\mathrm{T}} < 8$ GeV/$c$ (middle) and $p_{\mathrm{T}} > 8$ GeV/$c$ (right) as a function of self-normalized charged-particle multiplicity within $|\eta| < 0.9$ for the INEL>0 and V0M 0–0.1% event classes. The data are compared to PYTHIA 8 using different settings [69, 88], as well as EPOS4HQ [48–51], the 3-Pomeron CGC model [40, 41] and the CGC+ICEM model [38]. Lower panels show the ratios to the expectation from a linear increase. The vertical bars and boxes indicate the statistical and systematic uncertainties, respectively.

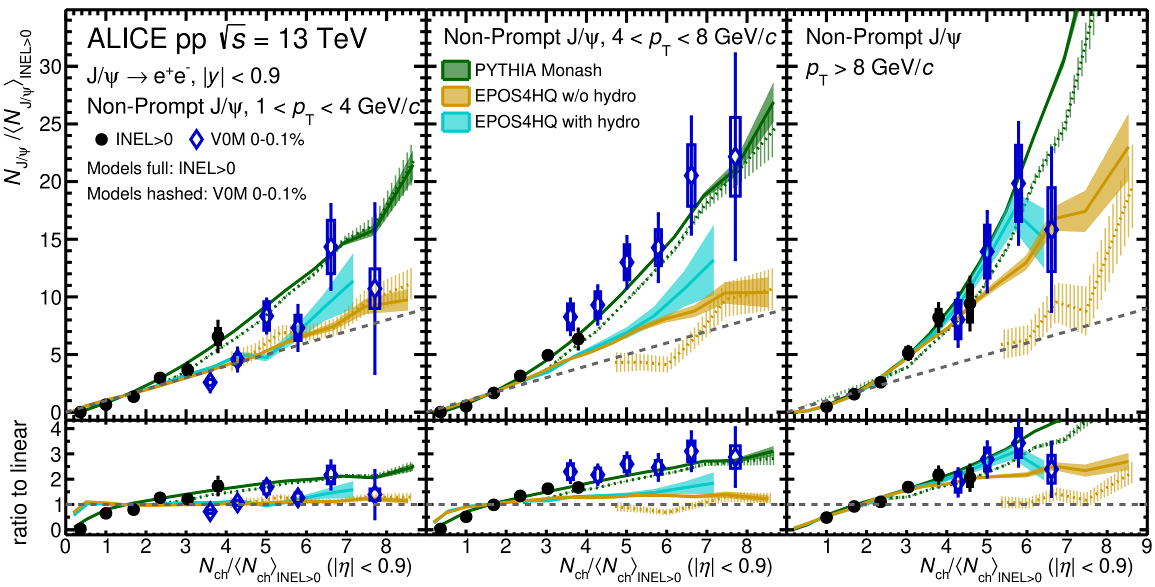


**Figure 6.** Non-prompt $J/\psi$ yield for $1 < p_{\mathrm{T}} < 4$ GeV/$c$ (left), $4 < p_{\mathrm{T}} < 8$ GeV/$c$ (middle) and $p_{\mathrm{T}} > 8$ GeV/$c$ (right) as a function of self-normalized charged-particle multiplicity within $|\eta| < 0.9$ for the INEL>0 and V0M 0–0.1% event classes. The data are compared to PYTHIA 8 using different settings [69, 88], as well as EPOS4HQ with and without hydrodynamics activated [48, 92]. Lower panels show the ratios to the expectation from a linear increase. The vertical bars and boxes indicate the statistical and systematic uncertainties, respectively.

JHEP07(2026)051

Figures 5 and 6 show the multiplicity dependence of the self-normalized yields separately in three $p_{\mathrm{T}}$ intervals ($1 < p_{\mathrm{T}} < 4$, $4 < p_{\mathrm{T}} < 8$, and $p_{\mathrm{T}} > 8$ GeV/$c$) for prompt and non-prompt J/$\psi$ mesons, respectively. In both cases, the slope of the multiplicity dependence is growing with increasing $p_{\mathrm{T}}$, as was previously seen also for inclusive J/$\psi$ mesons [20]. For all the $p_{\mathrm{T}}$ intervals, the slope is larger than 1. The increase of the slope is more pronounced between the first and second intervals than between the second and third. The HM trigger bias also seems noticeable in the data for non-prompt J/$\psi$ production in the lowest $p_{\mathrm{T}}$ interval.

The comparison to PYTHIA and EPOS4 calculations is qualitatively similar to the one for $p_{\mathrm{T}}$-integrated yields in the lowest two $p_{\mathrm{T}}$ intervals, with the exception of prompt J/$\psi$ production in the EPOS4 calculations. In the latter, no strong modification between low- and high-$p_{\mathrm{T}}$ J/$\psi$ yields is observed, leading to an overestimation at high multiplicity and low momentum. This could be explained by the more abundant number of charm quarks compared to higher momentum, which results in a larger combinatorial contribution. For $p_{\mathrm{T}} > 8$ GeV/$c$, all PYTHIA and EPOS4 calculations reproduce the data, although uncertainties are larger. The CGC-based calculations describe the data only partially, with a good description of the $1 < p_{\mathrm{T}} < 4$ GeV/$c$ results for the CGC+ICEM and of the $4 < p_{\mathrm{T}} < 8$ GeV/$c$ results for the 3-Pomeron implementation. For the other $p_{\mathrm{T}}$ intervals, these calculations either do not provide results or are in disagreement with the data.

### 4.2 Results as a function of multiplicity in azimuthal regions

In figure 7, the fractions of non-prompt J/$\psi$ mesons with $p_{\mathrm{T}} > 1$ GeV/$c$ are shown as a function of the self-normalized multiplicity measured in the toward (top-left), transverse (top-right) and away (bottom-left) azimuthal angle regions as defined in section 3.1. All regions present a hint of an increase of the non-prompt J/$\psi$ fraction as a function of multiplicity. A linear fit where the first point is excluded gives a significance compared to a flat trend of $2.9\sigma$ ($2.5\sigma$ and $2.4\sigma$) for the toward (transverse and away) region, respectively.

The PYTHIA calculations indicate a hierarchy of slopes for the increase of $f_{\mathrm{B}}$ with the event activity. It is the strongest in the toward region and the weakest in the transverse region. They also indicate an HM-trigger bias in the measurement using the toward multiplicity estimator comparable to the one for inclusive multiplicity, while this trigger bias is smaller in the transverse and away regions.

Figures 8 and 9 show the self-normalized yields as a function of the event activity in the three azimuthal angle regions for the prompt and non-prompt J/$\psi$ yields, respectively. In both cases, the increase with multiplicity is significantly stronger for the toward region compared to the other regions. This is presumably due to an autocorrelation with the particles produced along the J/$\psi$ direction in the same process. For the transverse and away multiplicity estimators, the J/$\psi$ yields at high multiplicity are only slightly higher than the $y = x$ reference.

The high-multiplicity trigger introduces a strong bias in the transverse and away multiplicities. This HM trigger bias is less significant in the toward region. It was pointed out that this trigger enhances multi-jet events with at least one jet in the V0 acceptance [95]. Therefore, at a given multiplicity in one region, the presence of a trigger could increase the multiplicity in the other regions, as was observed in the PYTHIA simulations. For the transverse and

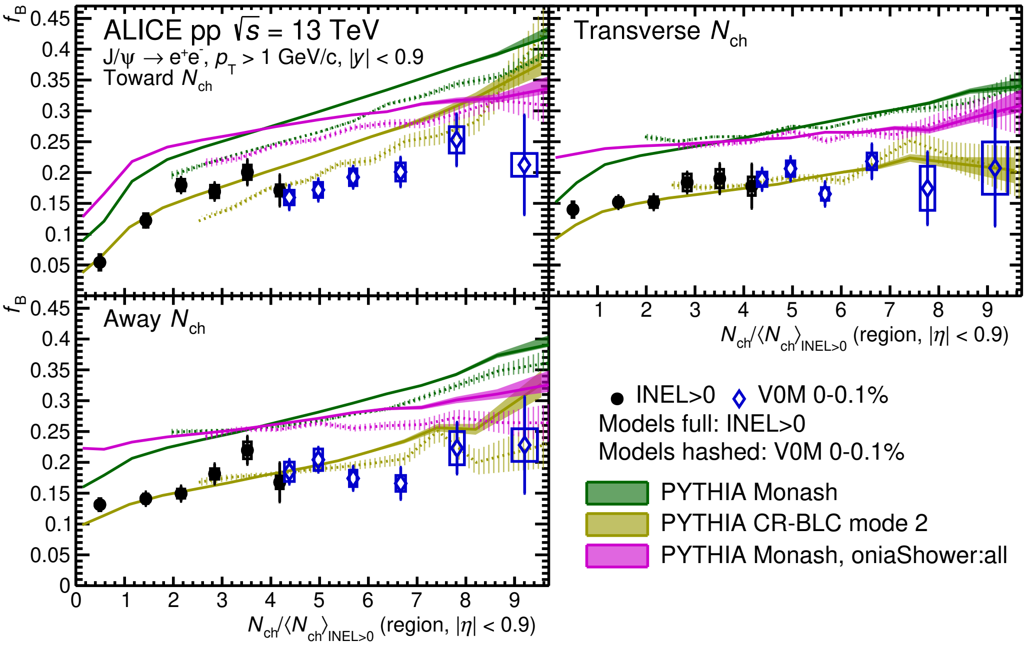


**Figure 7.** The fractions of J/$\psi$ mesons from beauty feed-down with $p_{\rm T} > 1$ GeV/$c$ as a function of the self-normalized charged-particle multiplicity in $|\eta| < 0.9$ in the toward (top-left), transverse (top-right), and away (bottom left) azimuthal regions with respect to the J/$\psi$ momentum direction. The data are shown separately for the INEL>0 and V0M 0–0.1% event classes and are compared to results from PYTHIA 8 simulations using different settings [47, 69, 88]. The vertical bars and boxes indicate the statistical and systematic uncertainties, respectively.

away regions, the toward-region multiplicity is increased, which could therefore increase the probability to find a J/$\psi$ meson in this region. This trigger bias, making the interpretation of the results harder, is stronger at lower multiplicity than at higher multiplicity, as can be seen also in the model curves. Since the J/$\psi$ meson is in the toward region, if the effect would come from an increased toward-region multiplicity, comparing INEL>0 and V0M 0–0.1% event classes at a similar toward multiplicity might not allow for a large HM trigger bias to appear.

Larger Poissonian fluctuations are expected for $N_{\rm ch,\ region}$ than for $N_{\rm ch}$, enhancing the number of events with large self-normalized $N_{\rm ch,\ region}$ compared to large self-normalized $N_{\rm ch}$. Therefore, the average $N_{\rm ch}/\langle N_{\rm ch}\rangle$ value in events where $N_{\rm ch,\ region}/\langle N_{\rm ch,\ region}\rangle$ is chosen as a given value $n_0$ is lower than $n_0$. Thus, measurements of the multiplicity in azimuthal regions, while the J/$\psi$ meson is measured in the full azimuth, cause in general a weaker increase compared to measurements using inclusive multiplicity. Therefore, the increase of the J/$\psi$ yields as a function of the transverse and away multiplicity could be stronger than the baseline of soft particle production. This is also confirmed by PYTHIA simulations, which predict that the increase of pion yields with the transverse and away multiplicity is weaker than linear. These PYTHIA simulations also show that, even for pions, the increase is stronger in the toward region compared to other regions. Therefore, the difference measured between the azimuthal regions could be partly caused by the definition of these regions and not only by additional autocorrelation effects for hard particle production.

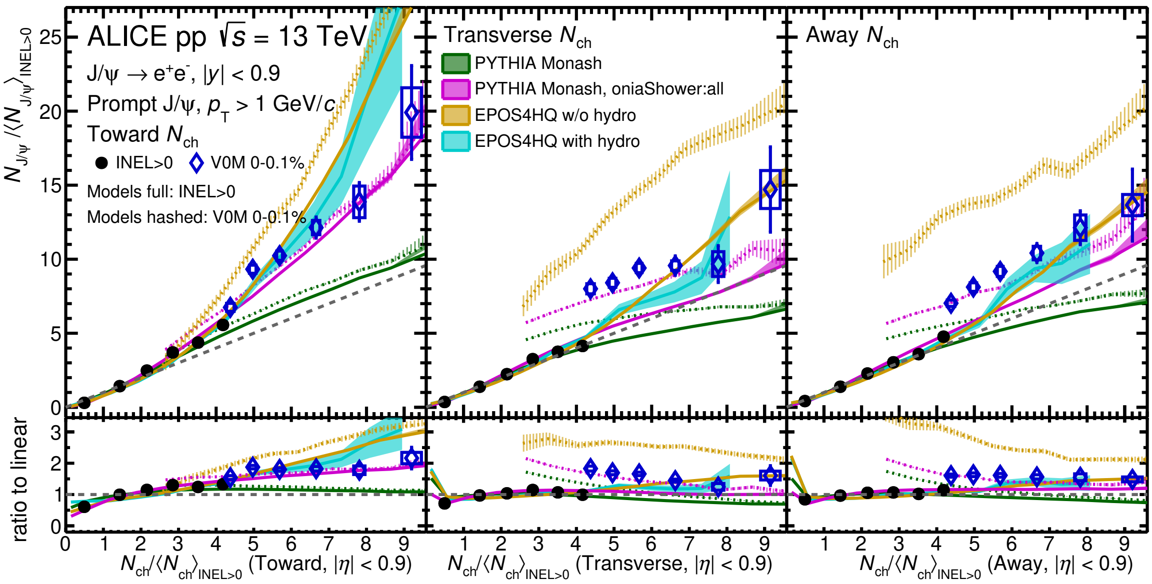


**Figure 8.** Self-normalized prompt J/$\psi$ yields with $p_{\mathrm{T}} > 1$ GeV/$c$ as a function of the self-normalized charged-particle multiplicity in $|\eta| < 0.9$ measured in the toward (left), transverse (middle), and away (right) azimuthal regions with respect to the J/$\psi$ momentum direction. The data are shown separately for the INEL>0 and V0M 0–0.1% event classes and are compared to PYTHIA 8 simulations using different settings [69, 88], as well as EPOS4HQ with and without hydrodynamics activated [48, 92]. The lower panels show the ratios to the expectation from a linear increase. The vertical bars and boxes indicate the statistical and systematic uncertainties, respectively.

Similar to the inclusive multiplicity case, PYTHIA Monash reproduces non-prompt J/$\psi$ yields in all regions while the oniaShower setting is necessary for reproducing the prompt yields. A stronger increase in the prompt yield as a function of toward multiplicity can be expected in oniaShower due to a modification of the production process and to the particles emitted in the parton shower. With the oniaShower process turned on, a stronger increase is also observed in the transverse region, possibly due to large angle radiations in the partonic shower. The transverse region might not be completely free of autocorrelations, even though they are smaller than in the other regions. In addition, oniaShower also predicts a stronger increase than Monash for the away region, which could be due to back-to-back jets. Contrary to the prompt case, for non-prompt J/$\psi$ production Monash predicts a stronger increase in the away region compared to the transverse region, possibly due to b$\overline{\mathrm{b}}$ correlations. However, here, the statistics do not allow a strong conclusion to be made on whether this is also the case in non-prompt data. At low $p_{\mathrm{T}}$, when the J/$\psi$ meson is not boosted, the J/$\psi$ decay daughters can also be included in other regions than the one towards the J/$\psi$ meson emission direction.

For the EPOS4 calculations, the prompt yield seems to be overestimated at high multiplicity in the toward region when hydrodynamic evolution is not activated. There is also a large difference when considering the V0M 0–0.1% event class, and the increase is slightly stronger for prompt J/$\psi$ production without hydrodynamics. For the transverse and away regions, EPOS4 also predicts a strong increase for prompt J/$\psi$ production as well as a strong trigger bias which largely overestimates the high-multiplicity data. In the non-prompt case, EPOS4

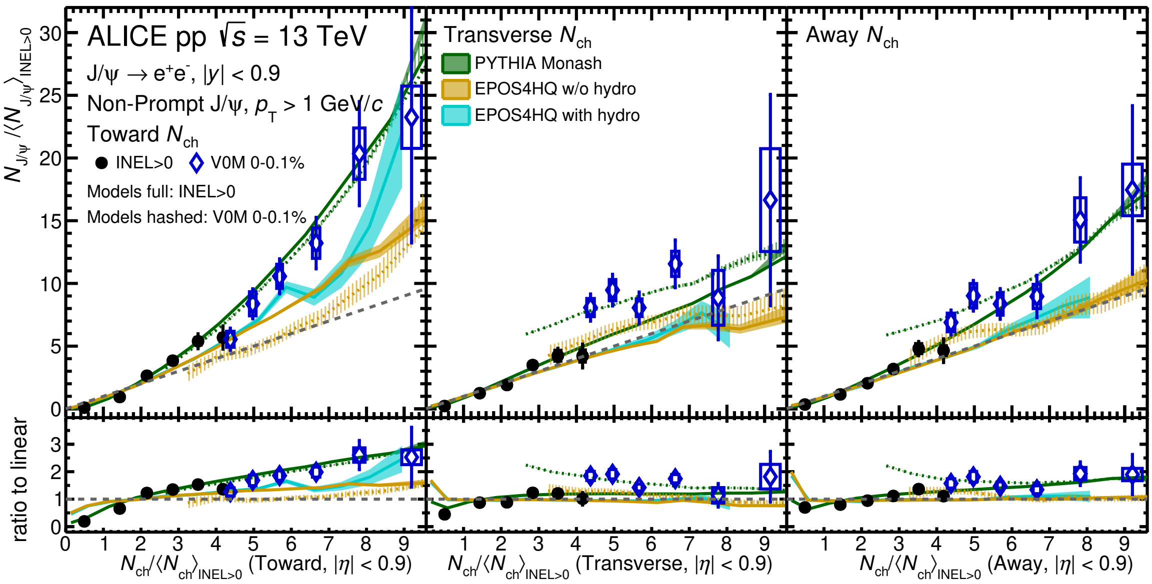


**Figure 9.** Self-normalized non-prompt $J/\psi$ yields with $p_T > 1$ GeV/$c$ as a function of the self-normalized charged-particle multiplicity in $|\eta| < 0.9$ measured in the toward (left), transverse (middle), and away (right) azimuthal regions with respect to the $J/\psi$ momentum direction. The data are shown separately for the INEL>0 and V0M 0–0.1% event classes and are compared to PYTHIA 8 simulations using different settings [69, 88], as well as EPOS4HQ with and without hydrodynamics activated [48, 92]. Lower panels show the ratios to the expectation from a linear increase. The vertical bars and boxes indicate the statistical and systematic uncertainties, respectively.

consistently underestimates the high-multiplicity yields for all regions. The hydrodynamic effect increases the correlation significantly only at high multiplicity in the toward region.

Finally, figures 10 (prompt) and 11 (non-prompt) show the $J/\psi$ yields as a function of multiplicity in the three azimuthal regions, separately for the three $p_T$ intervals. The strength of the dependence on the toward multiplicity for prompt $J/\psi$ production grows fast with the $J/\psi$ $p_T$, while only a moderate change is seen when using the transverse or away multiplicity. This suggests that the stronger increase of the multiplicity-dependent yields at higher $p_T$ could come from higher associated particle production, e.g. from a harder jet, rather than from underlying event properties. The $p_T$ dependence in the transverse and away region could also be affected by jet productions, such as the jets being more collimated or the more frequent occurrence of 3-jet topologies at high $p_T$. The additional presence of the $J/\psi$ decay daughters at low $p_T$ might also play a role. The opposite contributions of these effects when varying $p_T$ could hide a potential modification with increasing $p_T$ of the underlying event in the transverse region.

For non-prompt $J/\psi$ yields, a stronger increase at higher $p_T$ is measured for both the toward and away regions. It may also be present for the transverse region, although with a smaller magnitude. This is presumably related to the production process, connected to the strong back-to-back correlation of the beauty pair from which the non-prompt $J/\psi$ meson originates.

JHEP07(2026)051

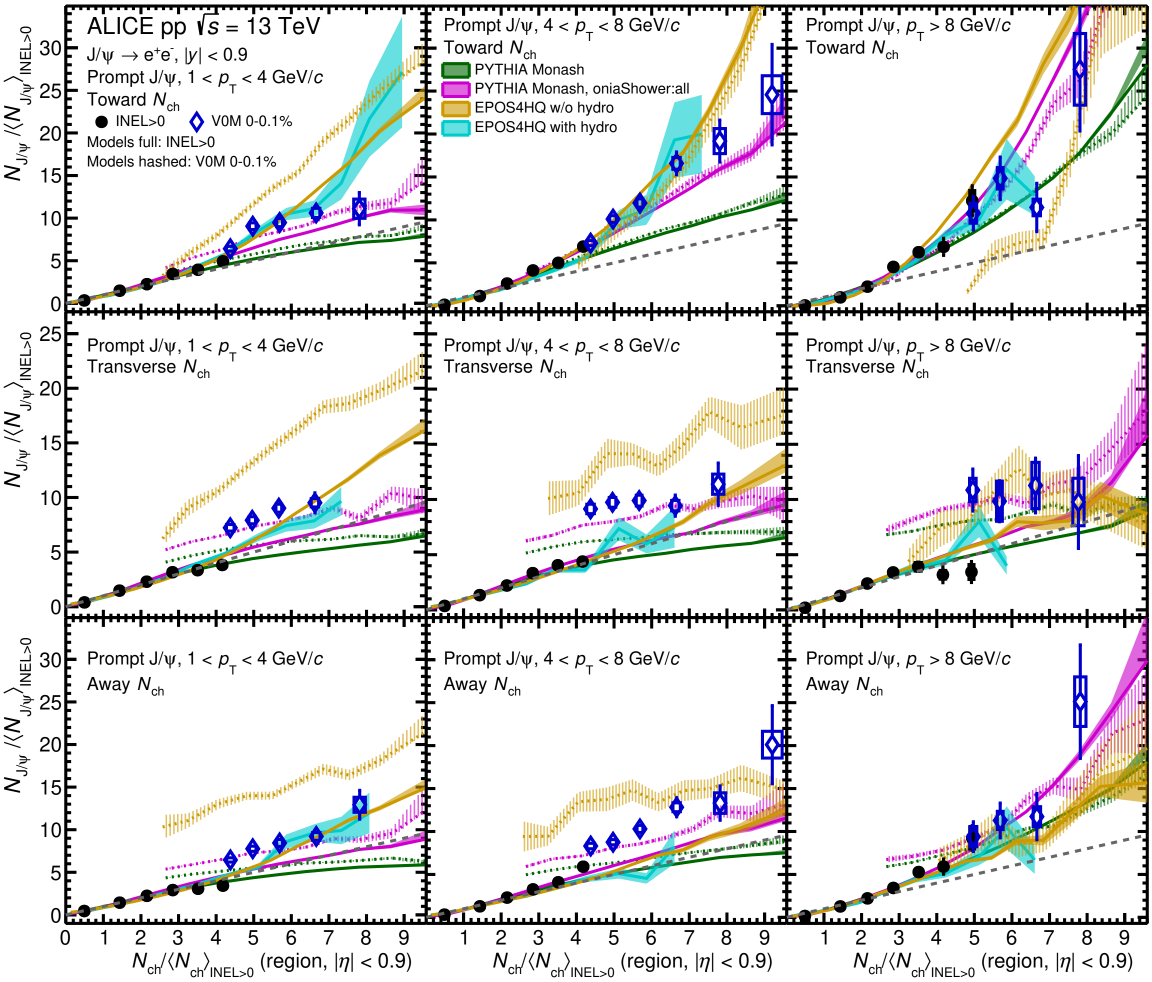


**Figure 10.** Self-normalized prompt $\mathrm{J}/\psi$ yields in the $p_{\mathrm{T}}$ intervals $1 < p_{\mathrm{T}} < 4$ GeV/$c$ (left column), $4 < p_{\mathrm{T}} < 8$ GeV/$c$ (middle column), and $p_{\mathrm{T}} > 8$ GeV/$c$ (right column) as a function of the self-normalized charged-particle multiplicity in $|\eta| < 0.9$ measured in toward (top row), transverse (middle row), and away (bottom row) azimuthal regions with respect to the $\mathrm{J}/\psi$ momentum direction. The data are shown separately for the INEL>0 and V0M 0–0.1% event classes and are compared to PYTHIA 8 simulations using different settings [69, 88], as well as EPOS4HQ with and without hydrodynamics activated [48, 92]. The dashed grey lines represent a linear increase with slope 1. The vertical bars and boxes indicate the statistical and systematic uncertainties, respectively.

Similar to the data, PYTHIA and EPOS4 calculations for prompt $\mathrm{J}/\psi$ production show a stronger increase of the correlation at higher $p_{\mathrm{T}}$ in the toward region, but not in the transverse region. In EPOS4, the non-prompt yields increase with multiplicity are stronger at higher $p_{\mathrm{T}}$ for all regions, which is not the case in PYTHIA. This could be due to the fact that the correlation between hard and soft scale is impacted by the saturation scale introduced in EPOS4. The effect of the saturation scale might influence all three regions as the saturation scale is a global event property.

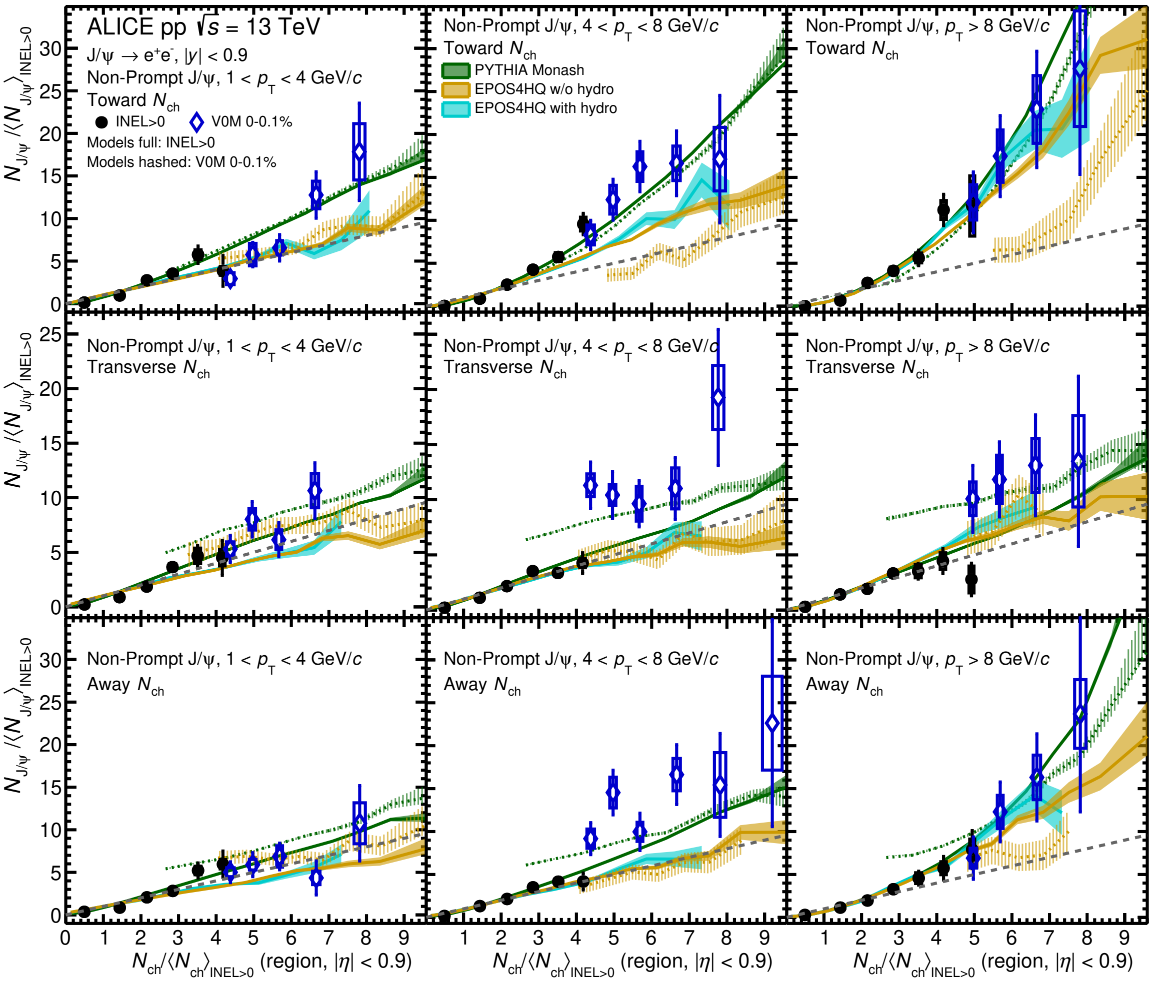


**Figure 11.** Self-normalized non-prompt J/$\psi$ yields in the $p_{\mathrm{T}}$ intervals $1 < p_{\mathrm{T}} < 4$ GeV/$c$ (left column), $4 < p_{\mathrm{T}} < 8$ GeV/$c$ (middle column), and $p_{\mathrm{T}} > 8$ GeV/$c$ (right column) as a function of the self-normalized charged-particle multiplicity in $|\eta| < 0.9$ measured in toward (top row), transverse (middle row), and away (bottom row) azimuthal regions with respect to the J/$\psi$ momentum direction. The data are shown separately for the INEL>0 and V0M 0–0.1% event classes and are compared to PYTHIA 8 simulations using different settings [69, 88], as well as EPOS4HQ with and without hydrodynamics activated [48, 92]. The dashed grey lines represent a linear increase with slope 1. The vertical bars and boxes indicate the statistical and systematic uncertainties, respectively.

### 4.3 J/$\psi$-to-D$^0$ ratio

The ratio between prompt J/$\psi$ and prompt D$^0$ yields is shown in figure 12 as a function of charged-particle multiplicity across several colliding systems. For pp collisions, the results are shown for integrated INEL>0 and V0M 0–0.1% event classes. Data for prompt D$^0$ and for other collision systems are taken from previous ALICE measurements in pp collisions at $\sqrt{s} = 13$ TeV [12], p–Pb collisions at $\sqrt{s_{\mathrm{NN}}} = 5.02$ TeV [96, 97], and Pb–Pb collisions at the same energy [52]. In the latter case, inclusive J/$\psi$ mesons are considered, and a momentum selection $p_{\mathrm{T}} > 0.15$ GeV/$c$ removes most of the contribution from photoproduction. The corresponding multiplicity values are also taken from previous ALICE measurements [99–101].

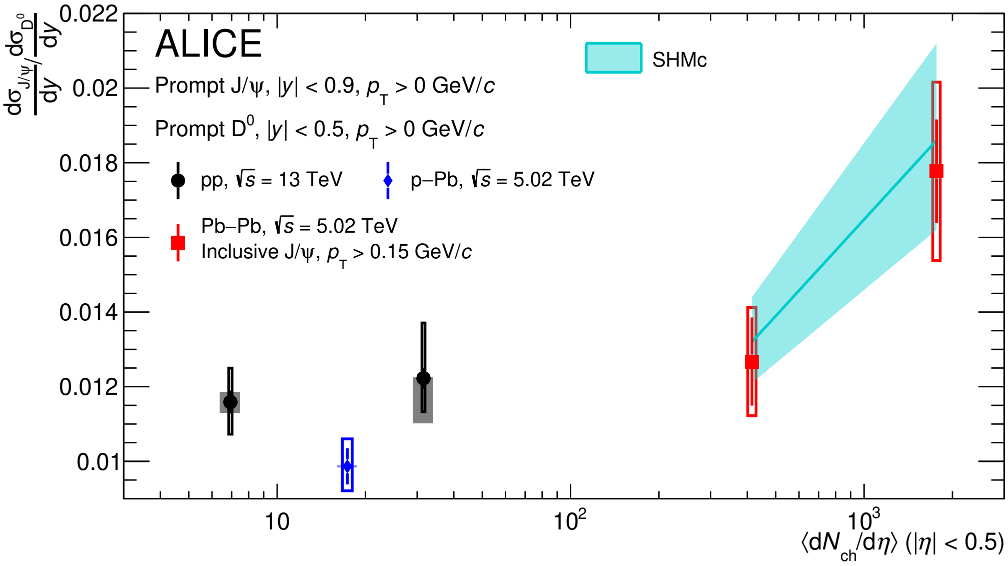


**Figure 12.** Ratio between the $p_{\mathrm{T}}$-integrated prompt J/$\psi$ and prompt $\mathrm{D}^0$ yields as a function of charged-particle multiplicity within $|\eta| < 0.5$ in several collision systems [52, 96, 97]. This is compared to the prediction from the Statistical Hadronization Model (SHMc) [98]. The vertical bars, empty and shaded boxes indicate the statistical, systematic and extrapolation uncertainties, respectively.

The prompt J/$\psi$ yield is extrapolated down to $p_{\mathrm{T}} = 0$ GeV/$c$. In order to do so, the inclusive yield is extracted for $p_{\mathrm{T}} < 1$ GeV/$c$, for both INEL>0 and V0M 0–0.1% classes, while the non-prompt yield for $p_{\mathrm{T}} < 1$ GeV/$c$ is subtracted from it. The non-prompt yield is estimated using PYTHIA with CR mode 2, scaled in order to reproduce the non-prompt yield in the data for $p_{\mathrm{T}} > 1$ GeV/$c$. The prompt yield with $p_{\mathrm{T}} < 1$ GeV/$c$ is then summed to the one with $p_{\mathrm{T}} > 1$ GeV/$c$. An extrapolation uncertainty is estimated by changing the model used for the extrapolation. The variations tested are: PYTHIA with Monash tune and CR mode 3, FONLL calculations with central value, upward and downward variations of the theory uncertainties. The maximum deviation considering all variations is assigned as extrapolation uncertainty in the INEL>0 case. In the V0M 0–0.1% case, because FONLL is not available, the envelope of all the PYTHIA variations is added in quadrature to the FONLL uncertainty for INEL>0. An uncertainty due to the scaling of the models for the non-prompt yield is also assigned. This is done by moving the data points used for the scaling by the sum in quadrature of statistical and systematic uncertainties. The tracking, MB trigger and luminosity uncertainties are assumed to cancel in the ratio.

In pp collisions, no modification of the ratio can be observed within uncertainties. The ratio in semicentral Pb–Pb collisions is compatible with the one in pp collisions within uncertainties, while the data suggest an increase for central collisions. The Pb–Pb data are described very well by the SHMc [98], which assumes that the J/$\psi$ and $\mathrm{D}^0$ mesons are produced at the QCD crossover phase boundary. While the increase in central Pb–Pb collisions could be due to regeneration of the J/$\psi$ from uncorrelated c and $\bar{\mathrm{c}}$ quarks, the current data, although they have large uncertainties, do not allow to conclude on such a regeneration in pp collisions at high multiplicity.

## 5 Summary and conclusions

The evolution of the yields of prompt and non-prompt J/$\psi$ mesons with charged-particle multiplicity has been measured in pp collisions at $\sqrt{s} = 13$ TeV. The charged-particle multiplicity is measured within $|\eta| < 0.9$, and separated in three azimuthal regions.

Both prompt and non-prompt J/$\psi$ self-normalized yields show a similar stronger-than-linear increase with self-normalized multiplicity. A hint of a slightly stronger increase for non-prompt J/$\psi$ yields is revealed by the evolution of the non-prompt fraction with multiplicity. The multiplicity dependence of the J/$\psi$ production is stronger at higher $p_T$ and when the multiplicity is evaluated in an azimuthal range towards the direction of the J/$\psi$ meson. In addition, the ratio between prompt J/$\psi$ and prompt $D^0$ yields does not show significant difference, within large uncertainties, between INEL>0 pp, high-multiplicity pp and semicentral Pb–Pb collisions. However, the measurements with the high-multiplicity (HM) trigger used to collect data at very high forward multiplicity show a significant bias in some cases. The results can nevertheless be interpreted by comparison with PYTHIA where a selection reproducing the effect of the trigger has been applied. PYTHIA calculations with several settings reproduce the results for non-prompt J/$\psi$ production. In contrast, for prompt J/$\psi$ production, the data are consistently underestimated by the Monash tune. The oniaShower setting is necessary to reproduce the measurement. CGC-based models are unable to reproduce the correlations in all the $p_T$ intervals, while EPOS4 calculations overestimate the prompt and underestimate the non-prompt J/$\psi$ results.

These measurements underline that autocorrelations with particles coming from the same production process as the J/$\psi$ meson are playing a role in the correlation between J/$\psi$ yields and multiplicity. Their role is significant for explaining the stronger increase of the multiplicity-dependent yields at higher $p_T$. The correlation remains also strong for the azimuthal region transverse to the J/$\psi$ direction. Therefore, it can be concluded that, in addition to the autocorrelations, there is also an effect on the correlation caused by the scales at play (relatively-hard for the J/$\psi$ meson, soft for the charged-particle multiplicity) in all regions.

During the Run 3 of the LHC, a larger dataset of pp collisions is being collected by ALICE without hardware triggers and with improved vertex pointing resolution. This will allow for more precise and less trigger-biased measurements of the multiplicity dependence of prompt and non-prompt J/$\psi$ production to be conducted in the future.

## Acknowledgments

We are grateful to E. Levin, M. Siddikov, R. Venugopalan, K. Watanabe, J. Zhao, and K. Werner for sending us the predictions of their models and for clarifications in this regard.

The ALICE Collaboration would like to thank all its engineers and technicians for their invaluable contributions to the construction of the experiment and the CERN accelerator teams for the outstanding performance of the LHC complex. The ALICE Collaboration gratefully acknowledges the resources and support provided by all Grid centres and the Worldwide LHC Computing Grid (WLCG) collaboration. The ALICE Collaboration acknowledges the following funding agencies for their support in building and running the ALICE detector: A.I. Alikhanyan National Science Laboratory (Yerevan Physics Institute) Foundation (ANSL), State Committee of Science and World Federation of Scientists (WFS), Armenia; Austrian Academy of Sciences, Austrian Science Fund (FWF): [M 2467-N36] and Nationalstiftung für Forschung, Technologie und Entwicklung, Austria; Ministry of Communications and High Technologies, National Nuclear Research Center, Azerbaijan; Rede Nacional de Física de Altas Energias (Renafae), Financiadora de Estudos e Projetos (Finep), Fundação de Amparo à Pesquisa do Estado de São Paulo (FAPESP) and The Sao Paulo Research Foundation (FAPESP), Brazil; Bulgarian Ministry of Education and Science, within the National Roadmap for Research Infrastructures 2020–2027 (object CERN), Bulgaria; Ministry of Education of China (MOEC), Ministry of Science & Technology of China (MSTC) and National Natural Science Foundation of China (NSFC), China; Ministry of Science and Education and Croatian Science Foundation, Croatia; Centro de Aplicaciones Tecnológicas y Desarrollo Nuclear (CEADEN), Cubaenergía, Cuba; Ministry of Education, Youth and Sports of the Czech Republic, Czech Republic; The Danish Council for Independent Research | Natural Sciences, the VILLUM FONDEN and Danish National Research Foundation (DNRF), Denmark; Helsinki Institute of Physics (HIP), Finland; Commissariat à l'Energie Atomique (CEA) and Institut National de Physique Nucléaire et de Physique des Particules (IN2P3) and Centre National de la Recherche Scientifique (CNRS), France; Bundesministerium für Forschung, Technologie und Raumfahrt (BMFTR) and GSI Helmholtzzentrum für Schwerionenforschung GmbH, Germany; National Research, Development and Innovation Office, Hungary; Department of Atomic Energy Government of India (DAE), Department of Science and Technology, Government of India (DST), University Grants Commission, Government of India (UGC) and Council of Scientific and Industrial Research (CSIR), India; National Research and Innovation Agency – BRIN, Indonesia; Istituto Nazionale di Fisica Nucleare (INFN), Italy; Japanese Ministry of Education, Culture, Sports, Science and Technology (MEXT) and Japan Society for the Promotion of Science (JSPS) KAKENHI, Japan; Consejo Nacional de Ciencia (CONACYT) y Tecnología, through Fondo de Cooperación Internacional en Ciencia y Tecnología (FONCICYT) and Dirección General de Asuntos del Personal Academico (DGAPA), Mexico; Nederlandse Organisatie voor Wetenschappelijk Onderzoek (NWO), Netherlands; The Research Council of Norway, Norway; Pontificia Universidad Católica del Perú, Peru; Ministry of Science and Higher Education, National Science Centre and WUT ID-UB, Poland; Korea Institute of Science and Technology Information and National Research Foundation of Korea (NRF), Republic of Korea; Ministry of Education and Scientific Research, Institute of Atomic Physics, Ministry of Research and Innovation and Institute of Atomic Physics and Universitatea Nationala de Stiinta si Tehnologie Politehnica Bucuresti, Romania; Ministerstvo skolstva, vyskumu, vyvoja a mladeze SR, Slovakia; National Research Foundation of South Africa, South Africa; Swedish Research Council (VR) and Knut & Alice Wallenberg Foundation (KAW), Sweden; European Organization for Nuclear Research, Switzerland; Suranaree University of Technology (SUT), National Science and Technology Development Agency (NSTDA) and National Science, Research and Innovation Fund (NSRF via PMU-B B05F650021), Thailand; Turkish Energy, Nuclear and Mineral Research Agency (TENMAK), Turkey; National Academy of Sciences of Ukraine, Ukraine; Science and Technology Facilities Council (STFC), United Kingdom; National Science Foundation of the United States of America (NSF) and United States Department of Energy, Office of Nuclear Physics (DOE NP),

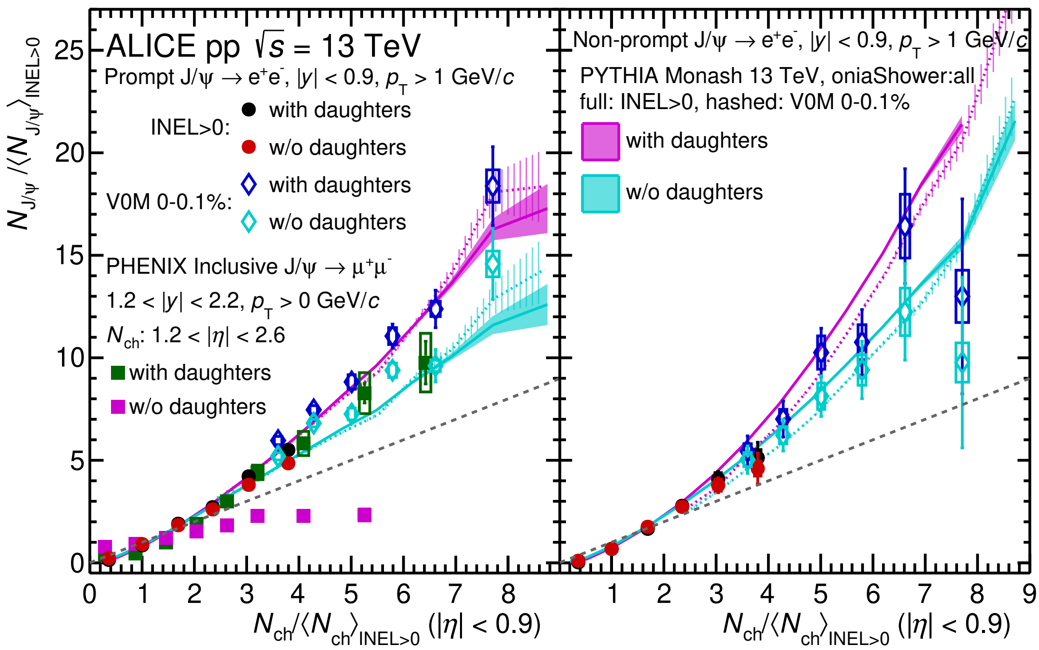


**Figure 13.** Self-normalized prompt (left) and non-prompt (right) J/$\psi$ yields with $p_{\mathrm{T}} > 1$ GeV/$c$ as a function of self-normalized charged-particle multiplicity within $|\eta| < 0.9$, in the INEL>0 (full markers) and V0M 0–0.1% (open markers) event classes. The case when the J/$\psi$ decay daughters are included in the multiplicity calculation is compared with the case when both J/$\psi$ decay daughters are removed from the multiplicity calculation. The yields are compared to PYTHIA 8 [46] using oniaShower:all settings. The dashed grey lines represent a linear increase with slope 1. The vertical bars and boxes indicate the statistical and systematic uncertainties, respectively. The prompt J/$\psi$ yields are also compared to the inclusive J/$\psi$ yields from the PHENIX collaboration [26].

United States of America. In addition, individual groups or members have received support from: FORTE project, reg. no. CZ.02.01.01/00/22_008/0004632, Czech Republic, co-funded by the European Union, Czech Republic; European Research Council (grant no. 950692), European Union; Deutsche Forschungs Gemeinschaft (DFG, German Research Foundation) "Neutrinos and Dark Matter in Astro- and Particle Physics" (grant no. SFB 1258), Germany; FAIR – Future Artificial Intelligence Research, funded by the NextGenerationEU program (Italy); CONVECS project, CUP C97H23001700002 FESR 2021-2027 program, Italy.

## A Discussion on the inclusion of the decay daughters in the multiplicity

When J/$\psi$ production and multiplicity are measured in the same rapidity region, the decay products of the J/$\psi$ meson may enter in the multiplicity count, potentially introducing a bias. In figure 13, the self-normalized yields of prompt and non-prompt J/$\psi$ mesons with $p_{\mathrm{T}} > 1$ GeV/$c$ are shown as a function of multiplicity, with and without including the J/$\psi$ decay daughters in the multiplicity calculation. Due to different multiplicity distributions at midrapidity, removing these two decay daughters has a different impact on INEL>0 and HM-triggered events. Therefore, for this figure only, when removing the J/$\psi$ decay daughters from the multiplicity, a multiplicity-dependent weight is applied to J/$\psi$ candidates in the

JHEP07(2026)051

HM sample. This weight is defined as

$$\frac{N_{\mathrm{evt}}^{\mathrm{HM}}\left(N_{\mathrm{trks}}^{\mathrm{w/o\ daughters}}\right)}{N_{\mathrm{evt}}^{\mathrm{INEL}>0}\left(N_{\mathrm{trks}}^{\mathrm{w/o\ daughters}}\right)}\frac{N_{\mathrm{evt}}^{\mathrm{INEL}>0}(N_{\mathrm{trks}})}{N_{\mathrm{evt}}^{\mathrm{HM}}(N_{\mathrm{trks}})}, \tag{A.1}$$

where $N_{\mathrm{evt}}$ represents the event multiplicity distributions, evaluated at the value of $N_{\mathrm{trks}}$ in the event containing the J/$\psi$ meson, either with or without excluding the J/$\psi$ decay daughters from $N_{\mathrm{trks}}$ calculation. This weight ensures that the HM trigger bias is similar when including and removing the J/$\psi$ decay daughters.

The decrease of the self-normalized yields when J/$\psi$ decay daughters are removed is found to be similar between prompt and non-prompt J/$\psi$ production. It is reproduced in PYTHIA, and is explained by the fact that the events with J/$\psi$ mesons are associated with a lower multiplicity value when the J/$\psi$ decay daughters are removed compared to when they are included. The total number of unbiased events with this lower multiplicity value is higher, thus reducing the J/$\psi$ yield per event. This shows the presence of autocorrelations, in this case brought about by the J/$\psi$ decay daughters. The results are also compared to the PHENIX measurement at $\sqrt{s} = 200$ GeV [26]. The impact of removing the J/$\psi$ decay daughters from the multiplicity on these results was found to be very significant at RHIC. However, at LHC energies, the observed effect is much smaller. This is explained by a higher average charged-particle multiplicity and a less steep decrease of the multiplicity distribution at LHC energies than at RHIC energies. The driving effects on the multiplicity distribution are the average number of MPIs and its fluctuations, which increase significantly from RHIC to LHC energies.

The multiplicity-dependent inclusive J/$\psi$ yield is very similar when the multiplicity is estimated directly at midrapidity and when it is selected at forward rapidity and converted to midrapidity multiplicity values [20]. The V0 estimator does not contain the J/$\psi$ decay daughters, but it could contain additional multiplicity indissociable from the J/$\psi$ production, such as a recoil jet. Thus, the bias present when estimating the multiplicity at midrapidity and including the J/$\psi$ decay daughters in the estimation could be small. In contrast, when removing the J/$\psi$ decay daughters from the multiplicity calculation, the additional multiplicity brought along with the presence of the J/$\psi$ meson is not accounted for. In a hypothetical baseline case for which hard and soft particle production would not differ, the measurement of J/$\psi$ production as a function of the total multiplicity would be expected to be linear. However, measuring J/$\psi$ yields only as a function of the multiplicity uncorrelated to itself would bias the measurement towards a weaker increase, and the baseline would not be linear.

Thus, all the measurements from section 4, as well as the calculations from MC generators, are shown with inclusion of the J/$\psi$ decay daughters in the multiplicity estimation. In models which are not MC generators, the J/$\psi$ decay daughters are not included or removed explicitly, and the impact of the absence of a clear treatment of these autocorrelations is not completely known.

## B Additional PYTHIA curves

Figure 14 shows the predictions from different PYTHIA settings (Monash [69], CR-BLC mode 2 [47], and oniaShower [88]) for prompt (left) and non-prompt (right) self-normalized

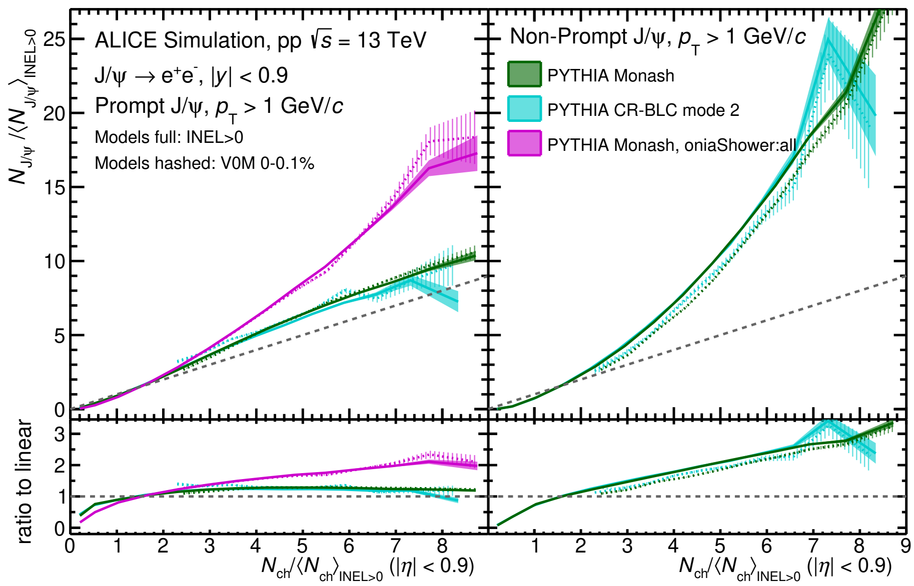


**Figure 14.** Self-normalized prompt (left) and non-prompt (right) J/$\psi$ yields with $p_{\mathrm{T}} > 1$ GeV/$c$ as a function of self-normalized charged-particle multiplicity at midrapidity from PYTHIA 8 simulations with different settings [47, 69, 88]. The yields are shown separately for the INEL>0 (full) and V0M 0–0.1% (hashed) event classes. Lower panels show the ratios to the expectation from a linear increase.

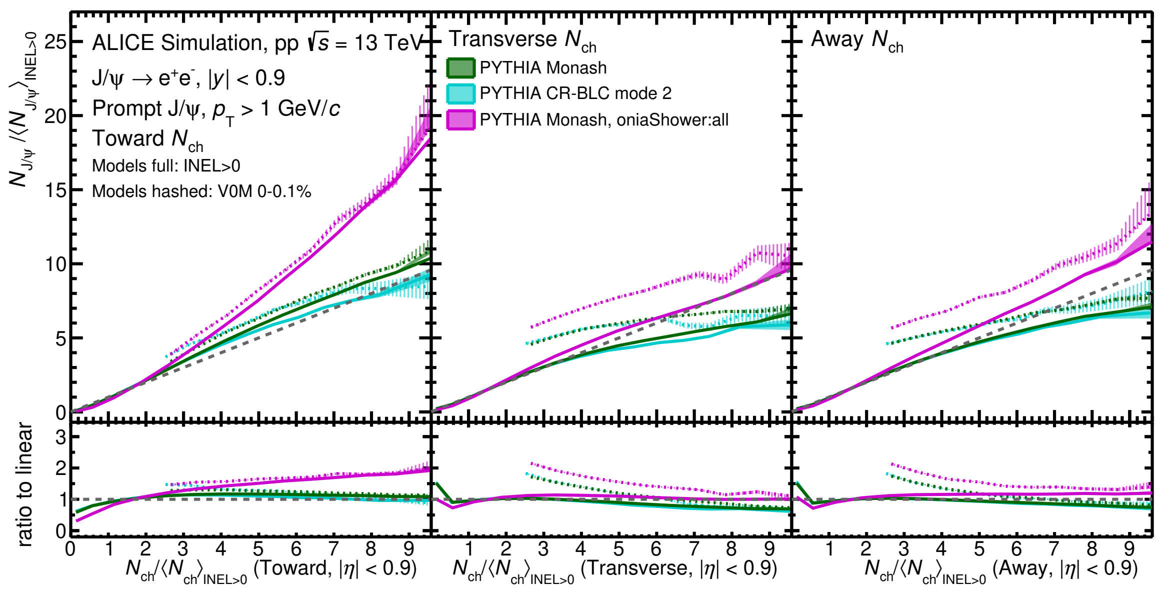


**Figure 15.** Self-normalized prompt J/$\psi$ yields with $p_{\mathrm{T}} > 1$ GeV/$c$, taken from PYTHIA 8 simulations with different settings [47, 69, 88], as a function of the self-normalized charged-particle multiplicity in $|\eta| < 0.9$ in the toward (left), transverse (middle), and away (right) azimuthal regions with respect to the J/$\psi$ momentum direction. The yields are shown separately for the INEL>0 (full) and V0M 0–0.1% (hashed) event classes. Lower panels show the ratios to the expectation from a linear increase.

yields. Figure 15 shows the PYTHIA comparison for prompt J/$\psi$ as a function of multiplicity in azimuthal regions. For all these predictions, CR-BLC mode 2 yields are found to be very close to Monash, while the oniaShower settings give significantly larger yields for prompt J/$\psi$.

**Data Availability Statement.** This manuscript has associated data in a HEPData repository at: https://www.hepdata.net/record/ins3142718.

**Code Availability Statement.** This manuscript has associated code/software in a data repository. The code/software used for the analysis is publicly available on the github repository, at the links https://github.com/alisw/AliRoot and https://github.com/alisw/AliPhysics/



## References

[1] Y.-Q. Ma and R. Vogt, *Quarkonium Production in an Improved Color Evaporation Model*, *Phys. Rev. D* **94** (2016) 114029 [arXiv:1609.06042] [INSPIRE].

[2] G.T. Bodwin, E. Braaten and G.P. Lepage, *Rigorous QCD analysis of inclusive annihilation and production of heavy quarkonium*, *Phys. Rev. D* **51** (1995) 1125 [*Erratum ibid.* **55** (1997) 5853] [hep-ph/9407339] [INSPIRE].

[3] Y.-Q. Ma and R. Venugopalan, *Comprehensive Description of J/$\psi$ Production in Proton-Proton Collisions at Collider Energies*, *Phys. Rev. Lett.* **113** (2014) 192301 [arXiv:1408.4075] [INSPIRE].

[4] M. Butenschoen and B.A. Kniehl, *Reconciling J/$\psi$ production at HERA, RHIC, Tevatron, and LHC with NRQCD factorization at next-to-leading order*, *Phys. Rev. Lett.* **106** (2011) 022003 [arXiv:1009.5662] [INSPIRE].

[5] V. Cheung and R. Vogt, *Production and polarization of prompt J/$\psi$ in the improved color evaporation model using the $k_T$-factorization approach*, *Phys. Rev. D* **98** (2018) 114029 [arXiv:1808.02909] [INSPIRE].

[6] S.P. Baranov and A.V. Lipatov, *Are there any challenges in the charmonia production and polarization at the LHC?*, *Phys. Rev. D* **100** (2019) 114021 [arXiv:1906.07182] [INSPIRE].

[7] L. Motyka and M. Sadzikowski, *On relevance of triple gluon fusion in J/$\psi$ hadroproduction*, *Eur. Phys. J. C* **75** (2015) 213 [arXiv:1501.04915] [INSPIRE].

[8] E. Levin and M. Siddikov, *J/$\psi$ production in hadron scattering: three-pomeron contribution*, *Eur. Phys. J. C* **79** (2019) 376 [arXiv:1812.06783] [INSPIRE].

[9] ALICE collaboration, *Charm production and fragmentation fractions at midrapidity in pp collisions at $\sqrt{s} = 13$ TeV*, *JHEP* **12** (2023) 086 [arXiv:2308.04877] [INSPIRE].

[10] ALICE collaboration, *Study of flavor dependence of the baryon-to-meson ratio in proton-proton collisions at $\sqrt{s} = 13$ TeV*, *Phys. Rev. D* **108** (2023) 112003 [arXiv:2308.04873] [INSPIRE].

[11] LHCb collaboration, *Enhanced production of $\Lambda_b^0$ baryons in high-multiplicity pp collisions at $\sqrt{s} = 13$ TeV*, *Phys. Rev. Lett.* **132** (2024) 081901 [arXiv:2310.12278] [INSPIRE].

[12] ALICE collaboration, *Observation of a multiplicity dependence in the $p_{\mathrm{T}}$-differential charm baryon-to-meson ratios in proton–proton collisions at $\sqrt{s} = 13$ TeV*, Phys. Lett. B **829** (2022) 137065 [arXiv:2111.11948] [INSPIRE].

[13] LHCb collaboration, *Evidence for modification of b quark hadronization in high-multiplicity pp collisions at $\sqrt{s} = 13$ TeV*, Phys. Rev. Lett. **131** (2023) 061901 [arXiv:2204.13042] [INSPIRE].

[14] J.F. Grosse-Oetringhaus and U.A. Wiedemann, *A Decade of Collectivity in Small Systems*, arXiv:2407.07484 [INSPIRE].

[15] ALICE collaboration, *Enhanced production of multi-strange hadrons in high-multiplicity proton-proton collisions*, Nature Phys. **13** (2017) 535 [arXiv:1606.07424] [INSPIRE].

[16] ALICE collaboration, *The ALICE experiment: a journey through QCD*, Eur. Phys. J. C **84** (2024) 813 [arXiv:2211.04384] [INSPIRE].

[17] ALICE collaboration, *Centrality dependence of strange particle production in Pb-Pb collisions at $\sqrt{s_{\mathrm{NN}}} = 5.02$ TeV*, arXiv:2511.10360 [INSPIRE].

[18] ALICE collaboration, *Strangeness enhancement at its extremes: multiple (multi-)strange hadron production in pp collisions at $\sqrt{s} = 5.02$ TeV*, arXiv:2511.10413 [INSPIRE].

[19] ALICE collaboration, *$J/\psi$ Production as a Function of Charged Particle Multiplicity in pp Collisions at $\sqrt{s} = 7$ TeV*, Phys. Lett. B **712** (2012) 165 [arXiv:1202.2816] [INSPIRE].

[20] ALICE collaboration, *Multiplicity dependence of $J/\psi$ production at midrapidity in pp collisions at $\sqrt{s} = 13$ TeV*, Phys. Lett. B **810** (2020) 135758 [arXiv:2005.11123] [INSPIRE].

[21] ALICE collaboration, *Forward rapidity $J/\psi$ production as a function of charged-particle multiplicity in pp collisions at $\sqrt{s} = 5.02$ and 13 TeV*, JHEP **06** (2022) 015 [arXiv:2112.09433] [INSPIRE].

[22] ALICE collaboration, *Multiplicity dependence of $\Upsilon$ production at forward rapidity in pp collisions at $\sqrt{s} = 13$ TeV*, Nucl. Phys. B **1011** (2025) 116786 [arXiv:2209.04241] [INSPIRE].

[23] ALICE collaboration, *Measurement of $\psi$(2S) production as a function of charged-particle pseudorapidity density in pp collisions at $\sqrt{s} = 13$ TeV and p–Pb collisions at $\sqrt{s_{\mathrm{NN}}} = 8.16$ TeV with ALICE at the LHC*, JHEP **06** (2023) 147 [arXiv:2204.10253] [INSPIRE].

[24] ALICE collaboration, *Multiplicity-dependent inclusive $J/\psi$ production at forward rapidity in pp collisions at $\sqrt{s} = 13$ TeV*, JHEP **07** (2025) 238 [arXiv:2504.00686] [INSPIRE].

[25] CMS collaboration, *Event Activity Dependence of Y(nS) Production in $\sqrt{s_{NN}} = 5.02$ TeV pPb and $\sqrt{s} = 2.76$ TeV pp Collisions*, JHEP **04** (2014) 103 [arXiv:1312.6300] [INSPIRE].

[26] PHENIX collaboration, *Multiplicity dependent $J/\psi$ and $\psi(2S)$ production at forward and backward rapidity in $p + p$ collisions at $\sqrt{s} = 200$ GeV*, Phys. Rev. D **112** (2025) L051103 [arXiv:2409.03728] [INSPIRE].

[27] STAR collaboration, *$J/\psi$ production cross section and its dependence on charged-particle multiplicity in $p + p$ collisions at $\sqrt{s} = 200$ GeV*, Phys. Lett. B **786** (2018) 87 [arXiv:1805.03745] [INSPIRE].

[28] STAR collaboration, *Measurements of $\Upsilon$ states production in p+p collisions at $\sqrt{s} = 500$ GeV with STAR: Cross sections, ratios, and multiplicity dependence*, Phys. Rev. D **112** (2025) 032004 [arXiv:2502.03769] [INSPIRE].

[29] ALICE collaboration, *Charged-particle production as a function of multiplicity and transverse spherocity in pp collisions at $\sqrt{s} = 5.02$ and 13 TeV*, Eur. Phys. J. C **79** (2019) 857 [arXiv:1905.07208] [INSPIRE].




JHEP07(2026)051

[30] ALICE collaboration, *Measurement of charm and beauty production at central rapidity versus charged-particle multiplicity in proton-proton collisions at $\sqrt{s} = 7$ TeV*, JHEP **09** (2015) 148 [arXiv:1505.00664] [INSPIRE].

[31] ALICE collaboration, *Inclusive and multiplicity dependent production of electrons from heavy-flavour hadron decays in pp and p–Pb collisions*, JHEP **08** (2023) 006 [arXiv:2303.13349] [INSPIRE].

[32] ALICE collaboration, *Measurements of the production of $W^{\pm}$ and $Z^0$ bosons in pp collisions at $\sqrt{s} = 13$ TeV*, arXiv:2602.22898 [INSPIRE].

[33] LHCb collaboration, *Multiplicity dependence of $\sigma_{\psi(2S)}/\sigma_{J/\psi}$ in pp collisions at $\sqrt{s} = 13$ TeV*, JHEP **05** (2024) 243 [arXiv:2312.15201] [INSPIRE].

[34] LHCb collaboration, *Measurement of the multiplicity dependence of $\Upsilon$ production ratios in pp collisions at $\sqrt{s} = 13$ TeV*, JHEP **05** (2025) 011 [arXiv:2501.12611] [INSPIRE].

[35] CMS collaboration, *Investigation into the event-activity dependence of $\Upsilon(nS)$ relative production in proton-proton collisions at $\sqrt{s} = 7$ TeV*, JHEP **11** (2020) 001 [arXiv:2007.04277] [INSPIRE].

[36] ALICE collaboration, *$J/\psi$ production as a function of charged-particle pseudorapidity density in p–Pb collisions at $\sqrt{s_{\rm NN}} = 5.02$ TeV*, Phys. Lett. B **776** (2018) 91 [arXiv:1704.00274] [INSPIRE].

[37] ALICE collaboration, *$J/\psi$ production as a function of charged-particle multiplicity in p–Pb collisions at $\sqrt{s_{\rm NN}} = 8.16$ TeV*, JHEP **09** (2020) 162 [arXiv:2004.12673] [INSPIRE].

[38] Y.-Q. Ma, P. Tribedy, R. Venugopalan and K. Watanabe, *Event engineering studies for heavy flavor production and hadronization in high multiplicity hadron-hadron and hadron-nucleus collisions*, Phys. Rev. D **98** (2018) 074025 [arXiv:1803.11093] [INSPIRE].

[39] F. Salazar, B. Schenke and A. Soto-Ontoso, *Accessing subnuclear fluctuations and saturation with multiplicity dependent $J/\psi$ production in p+p and p+Pb collisions*, Phys. Lett. B **827** (2022) 136952 [arXiv:2112.04611] [INSPIRE].

[40] E. Levin, I. Schmidt and M. Siddikov, *Multiplicity dependence of quarkonia production in the CGC approach*, Eur. Phys. J. C **80** (2020) 560 [arXiv:1910.13579] [INSPIRE].

[41] E. Gotsman and E. Levin, *High energy QCD: multiplicity dependence of quarkonia production*, Eur. Phys. J. C **81** (2021) 99 [arXiv:2008.10911] [INSPIRE].

[42] R. Terra and F.S. Navarra, *Charmonium production in high multiplicity pp collisions and the structure of the proton*, Phys. Rev. D **108** (2023) 054002 [arXiv:2306.14298] [INSPIRE].

[43] B.Z. Kopeliovich et al., *$J/\psi$ in high-multiplicity pp collisions: Lessons from pA collisions*, Phys. Rev. D **88** (2013) 116002 [arXiv:1308.3638] [INSPIRE].

[44] B.Z. Kopeliovich et al., *Heavy quarkonium in the saturated environment of high-multiplicity pp collisions*, Phys. Rev. D **101** (2020) 054023 [arXiv:1910.09682] [INSPIRE].

[45] E.G. Ferreiro and C. Pajares, *High multiplicity pp events and $J/\psi$ production at LHC*, Phys. Rev. C **86** (2012) 034903 [arXiv:1203.5936] [INSPIRE].

[46] C. Bierlich et al., *A comprehensive guide to the physics and usage of PYTHIA 8.3*, SciPost Phys. Codeb. **2022** (2022) 8 [arXiv:2203.11601] [INSPIRE].

[47] J.R. Christiansen and P.Z. Skands, *String Formation Beyond Leading Colour*, JHEP **08** (2015) 003 [arXiv:1505.01681] [INSPIRE].

[48] K. Werner, *Revealing a deep connection between factorization and saturation: New insight into modeling high-energy proton-proton and nucleus-nucleus scattering in the EPOS4 framework*, *Phys. Rev. C* **108** (2023) 064903 [arXiv:2301.12517] [INSPIRE].

[49] K. Werner and B. Guiot, *Perturbative QCD concerning light and heavy flavor in the EPOS4 framework*, *Phys. Rev. C* **108** (2023) 034904 [arXiv:2306.02396] [INSPIRE].

[50] K. Werner, *Core-corona procedure and microcanonical hadronization to understand strangeness enhancement in proton-proton and heavy ion collisions in the EPOS4 framework*, *Phys. Rev. C* **109** (2024) 014910 [arXiv:2306.10277] [INSPIRE].

[51] K. Werner, *Parallel scattering, saturation, and generalized Abramovskii-Gribov-Kancheli (AGK) theorem in the EPOS4 framework, with applications for heavy-ion collisions at* $\sqrt{s_{\rm NN}}$ *of 5.02 TeV and 200 GeV*, *Phys. Rev. C* **109** (2024) 034918 [arXiv:2310.09380] [INSPIRE].

[52] ALICE collaboration, *Measurements of inclusive J/ψ production at midrapidity and forward rapidity in Pb–Pb collisions at* $\sqrt{s_{\rm NN}} = 5.02$ *TeV*, *Phys. Lett. B* **849** (2024) 138451 [arXiv:2303.13361] [INSPIRE].

[53] LHCb collaboration, *J/ψ and* $D^0$ *production in* $\sqrt{s_{\rm NN}} = 68.5$ *GeV PbNe collisions*, *Eur. Phys. J. C* **83** (2023) 658 [arXiv:2211.11652] [INSPIRE].

[54] T. Martin, P. Skands and S. Farrington, *Probing Collective Effects in Hadronisation with the Extremes of the Underlying Event*, *Eur. Phys. J. C* **76** (2016) 299 [arXiv:1603.05298] [INSPIRE].

[55] ALICE collaboration, *Charged-particle production as a function of the relative transverse activity classifier in pp, p–Pb, and Pb–Pb collisions at the LHC*, *JHEP* **01** (2024) 056 [arXiv:2310.07490] [INSPIRE].

[56] ALICE collaboration, *Underlying Event properties in pp collisions at* $\sqrt{s} = 13$ *TeV*, *JHEP* **04** (2020) 192 [arXiv:1910.14400] [INSPIRE].

[57] S.G. Weber, A. Dubla, A. Andronic and A. Morsch, *Elucidating the multiplicity dependence of J/ψ production in proton–proton collisions with PYTHIA8*, *Eur. Phys. J. C* **79** (2019) 36 [arXiv:1811.07744] [INSPIRE].

[58] ALICE collaboration, *J/ψ-hadron correlations at midrapidity in pp collisions at* $\sqrt{s} = 13$ *TeV*, *JHEP* **07** (2025) 023 [arXiv:2409.04364] [INSPIRE].

[59] LHCb collaboration, *Study of J/ψ production in jets*, *Phys. Rev. Lett.* **118** (2017) 192001 [arXiv:1701.05116] [INSPIRE].

[60] ALICE collaboration, *Measurement of the charged-particle-jet transverse-momentum fraction carried by prompt and non-prompt J/ψ mesons in pp collisions at* $\sqrt{s} = 13$ *TeV*, arXiv:2602.22889 [INSPIRE].

[61] CMS collaboration, *Fragmentation of jets containing a prompt J/ψ meson in PbPb and pp collisions at* $\sqrt{s_{\rm NN}} = 5.02$ *TeV*, *Phys. Lett. B* **825** (2022) 136842 [arXiv:2106.13235] [INSPIRE].

[62] R. Bain et al., *NRQCD Confronts LHCb Data on Quarkonium Production within Jets*, *Phys. Rev. Lett.* **119** (2017) 032002 [arXiv:1702.05525] [INSPIRE].

[63] ALICE collaboration, *The ALICE experiment at the CERN LHC*, 2008 *JINST* **3** S08002 [INSPIRE].

[64] ALICE collaboration, *Performance of the ALICE Experiment at the CERN LHC*, *Int. J. Mod. Phys. A* **29** (2014) 1430044 [arXiv:1402.4476] [INSPIRE].

[65] ALICE collaboration, *Alignment of the ALICE Inner Tracking System with cosmic-ray tracks*, 2010 *JINST* **5** P03003 [arXiv:1001.0502] [INSPIRE].

[66] J. Alme et al., *The ALICE TPC, a large 3-dimensional tracking device with fast readout for ultra-high multiplicity events*, *Nucl. Instrum. Meth. A* **622** (2010) 316 [arXiv:1001.1950] [INSPIRE].

[67] ALICE collaboration, *Performance of the ALICE VZERO system*, 2013 *JINST* **8** P10016 [arXiv:1306.3130] [INSPIRE].

[68] ALICE collaboration, *The ALICE Transition Radiation Detector: construction, operation, and performance*, *Nucl. Instrum. Meth. A* **881** (2018) 88 [arXiv:1709.02743] [INSPIRE].

[69] P. Skands, S. Carrazza and J. Rojo, *Tuning PYTHIA 8.1: the Monash 2013 Tune*, *Eur. Phys. J. C* **74** (2014) 3024 [arXiv:1404.5630] [INSPIRE].

[70] R. Brun et al., *GEANT Detector Description and Simulation Tool*, CERN-W5013 (1994) [DOI:10.17181/CERN.MUHF.DMJ1] [INSPIRE].

[71] ALICE collaboration, *Multiplicity dependence of charged-particle production in pp, p–Pb, Xe–Xe and Pb–Pb collisions at the LHC*, *Phys. Lett. B* **845** (2023) 138110 [*Erratum ibid.* **853** (2024) 138700] [arXiv:2211.15326] [INSPIRE].

[72] T. Sjostrand, S. Mrenna and P.Z. Skands, *PYTHIA 6.4 Physics and Manual*, *JHEP* **05** (2006) 026 [hep-ph/0603175] [INSPIRE].

[73] D.J. Lange, *The EvtGen particle decay simulation package*, *Nucl. Instrum. Meth. A* **462** (2001) 152 [INSPIRE].

[74] E. Barberio and Z. Was, *PHOTOS: A Universal Monte Carlo for QED radiative corrections. Version 2.0*, *Comput. Phys. Commun.* **79** (1994) 291 [INSPIRE].

[75] ALICE collaboration, *The ALICE definition of primary particles*, ALICE-PUBLIC-2017-005 (2017) [INSPIRE].

[76] ALICE collaboration, *Transverse momentum spectra and nuclear modification factors of charged particles in pp, p–Pb and Pb–Pb collisions at the LHC*, *JHEP* **11** (2018) 013 [arXiv:1802.09145] [INSPIRE].

[77] G. D'Agostini, *A multidimensional unfolding method based on Bayes' theorem*, *Nucl. Instrum. Meth. A* **362** (1995) 487 [INSPIRE].

[78] ALICE collaboration, *Inclusive J/ψ production at midrapidity in pp collisions at $\sqrt{s} = 13$ TeV*, *Eur. Phys. J. C* **81** (2021) 1121 [arXiv:2108.01906] [INSPIRE].

[79] TMVA collaboration, *TMVA — Toolkit for Multivariate Data Analysis*, physics/0703039 [INSPIRE].

[80] Particle Data Group collaboration, *Review of particle physics*, *Phys. Rev. D* **110** (2024) 030001 [INSPIRE].

[81] ALICE collaboration, *Measurement of beauty and charm production in pp collisions at $\sqrt{s} = 5.02$ TeV via non-prompt and prompt D mesons*, *JHEP* **05** (2021) 220 [arXiv:2102.13601] [INSPIRE].

[82] ALICE collaboration, *Measurement of prompt J/ψ and beauty hadron production cross sections at mid-rapidity in pp collisions at $\sqrt{s} = 7$ TeV*, *JHEP* **11** (2012) 065 [arXiv:1205.5880] [INSPIRE].

[83] ALICE collaboration, *Prompt and non-prompt J/ψ production cross section at midrapidity in proton-proton collisions at* $\sqrt{s} = 5.02$ *and* 13 *TeV*, *JHEP* **03** (2022) 190 [arXiv:2108.02523] [INSPIRE].

[84] ALICE collaboration, *Inclusive* $\psi(2S)$ *production at midrapidity in pp collisions at* $\sqrt{s} = 13$ *TeV*, arXiv:2602.22848 [INSPIRE].

[85] B. Malaescu, *An iterative, dynamically stabilized method of data unfolding*, arXiv:0907.3791 [INSPIRE].

[86] M. Cacciari, M. Greco and P. Nason, *The* $p_T$ *spectrum in heavy-flavour hadroproduction*, *JHEP* **05** (1998) 007 [hep-ph/9803400] [INSPIRE].

[87] M. Cacciari et al., *Theoretical predictions for charm and bottom production at the LHC*, *JHEP* **10** (2012) 137 [arXiv:1205.6344] [INSPIRE].

[88] N. Cooke, P. Ilten, L. Lönnblad and S. Mrenna, *Non-relativistic quantum chromodynamics in parton showers*, *Eur. Phys. J. C* **84** (2024) 432 [arXiv:2312.05203] [INSPIRE].

[89] R. Baier and R. Ruckl, *Hadronic Collisions: A Quarkonium Factory*, *Z. Phys. C* **19** (1983) 251 [INSPIRE].

[90] P.L. Cho and A.K. Leibovich, *Color octet quarkonia production. 2*, *Phys. Rev. D* **53** (1996) 6203 [hep-ph/9511315] [INSPIRE].

[91] P. Nason et al., *Bottom production*, in the proceedings of the *Workshop on Standard Model Physics (and more) at the LHC (First Plenary Meeting)*, Geneva, Switzerland, May 25–26 (1999) [DOI:10.5170/CERN-2000-004.231] [hep-ph/0003142] [INSPIRE].

[92] J. Zhao, J. Aichelin, P.B. Gossiaux and K. Werner, *Heavy flavor as a probe of hot QCD matter produced in proton-proton collisions*, *Phys. Rev. D* **109** (2024) 054011 [arXiv:2310.08684] [INSPIRE].

[93] J. Zhao et al., *Heavy-flavor hadron production in relativistic heavy ion collisions at energies available at BNL RHIC and at the CERN LHC in the EPOS4HQ framework*, *Phys. Rev. C* **110** (2024) 024909 [arXiv:2401.17096] [INSPIRE].

[94] J. Zhao, J. Aichelin, P.B. Gossiaux and K. Werner, *Correlations between heavy mesons and the creation of the charmonia, bottomonia, and* $B_c$ *mesons in high energy pp collisions*, *Phys. Rev. D* **113** (2026) 116022 [arXiv:2511.08796] [INSPIRE].

[95] ALICE collaboration, *Search for jet quenching effects in high-multiplicity pp collisions at* $\sqrt{s} = 13$ *TeV via di-jet acoplanarity*, *JHEP* **05** (2024) 229 [arXiv:2309.03788] [INSPIRE].

[96] ALICE collaboration, *Measurement of prompt* $D^0$, $D^+$, $D^{*+}$, *and* $D_s^+$ *production in p-Pb collisions at* $\sqrt{s_{\rm NN}} = 5.02$ *TeV*, *JHEP* **12** (2019) 092 [arXiv:1906.03425] [INSPIRE].

[97] ALICE collaboration, *Inclusive, prompt and non-prompt J/ψ production at midrapidity in p-Pb collisions at* $\sqrt{s_{\rm NN}} = 5.02$ *TeV*, *JHEP* **06** (2022) 011 [arXiv:2105.04957] [INSPIRE].

[98] A. Andronic et al., *The multiple-charm hierarchy in the statistical hadronization model*, *JHEP* **07** (2021) 035 [arXiv:2104.12754] [INSPIRE].

[99] ALICE collaboration, *Pseudorapidity distributions of charged particles as a function of mid- and forward rapidity multiplicities in pp collisions at* $\sqrt{s} = 5.02$, 7 *and* 13 *TeV*, *Eur. Phys. J. C* **81** (2021) 630 [arXiv:2009.09434] [INSPIRE].

[100] ALICE collaboration, *Pseudorapidity density of charged particles in p + Pb collisions at* $\sqrt{s_{NN}} = 5.02$ *TeV*, *Phys. Rev. Lett.* **110** (2013) 032301 [arXiv:1210.3615] [INSPIRE].

[101] ALICE collaboration, *Centrality Dependence of the Charged-Particle Multiplicity Density at Midrapidity in Pb-Pb Collisions at* $\sqrt{s_{NN}} = 5.02$ *TeV*, *Phys. Rev. Lett.* **116** (2016) 222302 [arXiv:1512.06104] [INSPIRE].

[102] https://www.hepdata.net/record/ins3142718.

[103] https://github.com/alisw/AliRoot.

[104] https://github.com/alisw/AliPhysics/.

## The ALICE collaboration

D.A.H. Abdallah[134], I.J. Abualrob[112], S. Acharya[49], K. Agarwal[23,a], G. Aglieri Rinella[32], L. Aglietta[24], N. Agrawal[25], Z. Ahammed[132], S. Ahmad[15], I. Ahuja[36], Z. Akbar[79], V. Akishina[38], M. Al-Turany[94], B. Alessandro[55], A.R. Alfarasyi[101], R. Alfaro Molina[66], B. Ali[15], A. Alici[25,†], J. Alme[20], G. Alocco[24], T. Alt[63], I. Altsybeev[92], C. Andrei[44], N. Andreou[111], A. Andronic[123], M. Angeletti[32], V. Anguelov[91], F. Antinori[53], P. Antonioli[50], N. Apadula[71], H. Appelshäuser[63], S. Arcelli[25,†], R. Arnaldi[55], I.C. Arsene[19], M. Arslandok[135], A. Augustinus[32], R. Averbeck[94], M.D. Azmi[15], H. Baba[121], A.R.J. Babu[134], A. Badalà[52], J. Bae[100], Y. Bae[100], Y.W. Baek[100], X. Bai[116], R. Bailhache[63], Y. Bailung[125], R. Bala[88], A. Baldisseri[127], B. Balis[2], S. Bangalia[114], Z. Banoo[88], V. Barbasova[36], F. Barile[31], L. Barioglio[55], M. Barlou[24], B. Barman[40], G.G. Barnaföldi[45], L.S. Barnby[111], E. Barreau[99], V. Barret[124], L. Barreto[106], K. Barth[32], E. Bartsch[63], N. Bastid[124], G. Batigne[99], D. Battistini[34,92], B. Batyunya[139], L. Baudino[24,b], D. Bauri[46], J.L. Bazo Alba[98], I.G. Bearden[80], P. Becht[94], D. Behera[47,77], S. Behera[46], M.A.C. Behling[63], I. Belikov[126], V.D. Bella[126], F. Bellini[25], R. Bellwied[112], L.G.E. Beltran[105], Y.A.V. Beltran[43], G. Bencedi[45], O. Benchikhi[73], A. Bensaoula[112], S. Beole[24], A. Berdnikova[91], L. Bergmann[71], L. Bernardinis[23], L. Betev[32], P.P. Bhaduri[132], T. Bhalla[87], A. Bhasin[88], B. Bhattacharjee[40], L. Bianchi[24], J. Bielčík[34], J. Bielčíková[83], A. Bilandzic[92], A. Binoy[114], G. Biro[45], S. Biswas[4], M.B. Blidaru[94], N. Bluhme[38], C. Blume[63], F. Bock[84], T. Bodova[20], L. Boldizsár[45], M. Bombara[36], P.M. Bond[32], G. Bonomi[54,131], H. Borel[127], A. Borissov[139], A.G. Borquez Carcamo[91], E. Botta[24], N. Bouchhar[17], Y.E.M. Bouziani[63], D.C. Brandibur[62], L. Bratrud[63], P. Braun-Munzinger[94], M. Bregant[106], M. Broz[34], G.E. Bruno[31,93], V.D. Buchakchiev[35], M.D. Buckland[82], H. Buesching[63], S. Bufalino[29], P. Buhler[73], N. Burmasov[139], Z. Buthelezi[67,120], A. Bylinkin[20], J.C. Cabanillas Noris[105], M.F.T. Cabrera[112], H. Caines[135], A. Caliva[28], E. Calvo Villar[98], J.M.M. Camacho[105], P. Camerini[23], M.T. Camerlingo[49], F.D.M. Canedo[106], S. Cannito[23], S.L. Cantway[135], M. Carabas[109], F. Carnesecchi[32], C. Carr[97], L.A.D. Carvalho[106], J. Castillo Castellanos[127], M. Castoldi[32], F. Catalano[112], S. Cattaruzzi[23], R. Cerri[24], I. Chakaberia[71], P. Chakraborty[133], J.W.O. Chan[112], S. Chandra[132], S. Chapeland[32], M. Chartier[115], S. Chattopadhay[132], M. Chen[39], T. Cheng[6], M.I. Cherciu[62], C. Cheshkov[125], D. Chiappara[27], V. Chibante Barroso[32], D.D. Chinellato[73], F. Chinu[24], E.S. Chizzali[92,c], J. Cho[57], S. Cho[57], P. Chochula[32], Z.A. Chochulska[133,d], P. Christakoglou[81], P. Christiansen[72], T. Chujo[122], B. Chytla[133], M. Ciacco[24], C. Cicalo[51], G. Cimador[24,32], F. Cindolo[50], F. Colamaria[49], D. Colella[31], A. Colelli[31], M. Colocci[25], M. Concas[32], G. Conesa Balbastre[70], Z. Conesa del Valle[128], G. Contin[23], J.G. Contreras[34], M.L. Coquet[99], P. Cortese[55,130], M.R. Cosentino[108], F. Costa[32], S. Costanza[21], P. Crochet[124], M.M. Czarnynoga[133], A. Dainese[53], E. Dall'occo[32], G. Dange[38], M.C. Danisch[16], A. Danu[62], A. Daribayeva[38], P. Das[32], S. Das[4], A.R. Dash[123], S. Dash[46], A. De Caro[28], G. de Cataldo[49], J. de Cuveland[38], A. De Falco[22], D. De Gruttola[28], N. De Marco[55], C. De Martin[23], S. De Pasquale[28], G.G.A. de Souza[106,e], R. Deb[131], R. Del Grande[34], L. Dello Stritto[32], P. Dhankher[18], D. Di Bari[31], M. Di Costanzo[29], A. Di Mauro[32], B. Di Ruzza[49,129,†], B. Diab[32], Y. Ding[6], J. Ditzel[63], R. Divià[32], U. Dmitrieva[55],

JHEP07(2026)051

A. Dobrin[62], B. Dönigus[63], L. Döpper[41], L. Drzensla[2], J.M. Dubinski[133], A. Dubla[94], P. Dupieux[124], N. Dzalaiova[13], T.M. Eder[123], E.C. Ege[63], R.J. Ehlers[71], F. Eisenhut[63], R. Ejima[89], D. Elia[49], B. Erazmus[99], F. Ercolessi[25], B. Espagnon[128], G. Eulisse[32], D. Evans[97], L. Fabbietti[92], G. Fabbri[50], M. Faggin[32], J. Faivre[70], W. Fan[112], T. Fang[6], A. Fantoni[48], A. Feliciello[55], W. Feng[6], A. Fernández Téllez[43], B. Fernando[134], L. Ferrandi[106], A. Ferrero[127], C. Ferrero[55,f], A. Ferretti[24], F.M. Fionda[51], A.N. Flores[104], S. Foertsch[67], I. Fokin[91], U. Follo[55,f], R. Forynski[111], E. Fragiacomo[56], H. Fribert[92], J.M. Friedrich[92], U. Fuchs[32], D. Fuligno[23], N. Funicello[28], C. Furget[70], T. Fusayasu[95], J.J. Gaardhøje[80], M. Gagliardi[24], A.M. Gago[98], T. Gahlaut[46], C.D. Galvan[105], S. Gami[77], C. Garabatos[94], J.M. Garcia[43], E. Garcia-Solis[9], S. Garetti[128], C. Gargiulo[32], P. Gasik[94], A. Gautam[114], M.B. Gay Ducati[65], M. Germain[99], R.A. Gernhaeuser[92], M. Giacalone[32], G. Gioachin[29], S.K. Giri[132], P. Giubellino[55], P. Giubilato[27], P. Glässel[91], E. Glimos[119], M.G.F.S.A. Gomes[91], L. Gonella[23], V. Gonzalez[134], M. Gorgon[2], K. Goswami[47], S. Gotovac[33], V. Grabski[66], L.K. Graczykowski[133], E. Grecka[83], A. Grelli[58], C. Grigoras[32], S. Grigoryan[1,139], O.S. Groettvik[32], M. Gronbeck[41], F. Grosa[32], S. Gross-Bölting[94], J.F. Grosse-Oetringhaus[32], R. Grosso[94], D. Grund[34], N.A. Grunwald[91], R. Guernane[70], M. Guilbaud[99], K. Gulbrandsen[80], J.K. Gumprecht[73], T. Gündem[63], T. Gunji[121], J. Guo[10], W. Guo[6], A. Gupta[88], R. Gupta[88], R. Gupta[47], K. Gwizdziel[133], L. Gyulai[45], T. Hachiya[75], C. Hadjidakis[128], F.U. Haider[88], S. Haidlova[34], M. Haldar[4], W. Ham[100], H. Hamagaki[74], Y. Han[137], R. Hannigan[104], J. Hansen[72], J.W. Harris[135], A. Harton[9], M.V. Hartung[63], A. Hasan[118], H. Hassan[113], D. Hatzifotiadou[50], P. Hauer[41], L.B. Havener[135], E. Hellbär[32], H. Helstrup[37], M. Hemmer[63], S.G. Hernandez[112], G. Herrera Corral[8], K.F. Hetland[37], B. Heybeck[63], H. Hillemanns[32], B. Hippolyte[126], I.P.M. Hobus[81], F.W. Hoffmann[38], B. Hofman[58], Y. Hong[57], A. Horzyk[2], Y. Hou[11,94], P. Hristov[32], L.M. Huhta[113], T.J. Humanic[85], V. Humlova[34], M. Husar[86], A. Hutson[112], D. Hutter[38], M.C. Hwang[18], M. Inaba[122], A. Isakov[81], T. Isidori[114], M.S. Islam[46], M. Ivanov[94], M. Ivanov[13], K.E. Iversen[72], M. Jablonski[2], B. Jacak[18,71], N. Jacazio[25], P.M. Jacobs[71], A. Jadlovska[102], S. Jadlovska[102], S. Jaelani[79], J.N. Jager[63], C. Jahnke[107], M.J. Jakubowska[133], E.P. Jamro[2], D.M. Janik[34], M.A. Janik[133], C.A. Jauch[94], S. Ji[16], Y. Ji[94], S. Jia[80], T. Jiang[10], A.A.P. Jimenez[64], S. Jin[10], F. Jonas[71], D.M. Jones[115], J.M. Jowett[32,94], J. Jung[63], M. Jung[63], A. Junique[32], J. Juračka[34], J. Kaewjai[101,115], A. Kaiser[32,94], P. Kalinak[59], A. Kalweit[32], H. Kang[12], A. Karasu Uysal[136], N. Karatzenis[97], T. Karavicheva[139], M.J. Karwowska[133], V. Kashyap[77], M. Keil[32], B. Ketzer[41], J. Keul[63], S.S. Khade[47], A. Khuntia[50], Z. Khuranova[63], B. Kileng[37], B. Kim[100], D. Kim[100], D.J. Kim[113], E.J. Kim[68], G. Kim[57], H. Kim[57], J. Kim[137], J. Kim[57], J. Kim[137], J. Kim[32], M. Kim[18], S. Kim[17], T. Kim[137], J.T. Kinner[123], I. Kisel[38], A. Kisiel[133], J.L. Klay[5], J. Klein[32], S. Klein[71], C. Klein-Bösing[123], M. Kleiner[63], A. Kluge[32], M.B. Knuesel[135], C. Kobdaj[101], R. Kohara[121], A. Kondratyev[139], J. Konig[63], P.J. Konopka[32], G. Kornakov[133], M. Korwieser[92], C. Koster[81], A. Kotliarov[83], N. Kovacic[86], M. Kowalski[103], V. Kozhuharov[35], G. Kozlov[38], I. Králik[59], A. Kravčáková[36], M.A. Krawczyk[32], L. Krcal[32], F. Krizek[83], K. Krizkova Gajdosova[34], C. Krug[65], M. Krüger[63], E. Kryshen[139], V. Kučera[57], C. Kuhn[126], D. Kumar[132],

L. Kumar[87], N. Kumar[87], S. Kumar[49], S. Kundu[32], M. Kuo[122], P. Kurashvili[76], S. Kurita[89], S. Kushpil[83], A. Kuznetsov[139], M.J. Kweon[57], Y. Kwon[137], S.L. La Pointe[38], P. La Rocca[26], A. Lakrathok[101], S. Lambert[99], A.R. Landou[70], R. Langoy[118], P. Larionov[32], E. Laudi[32], L. Lautner[92], R.A.N. Laveaga[105], R. Lavicka[73], R. Lea[54,131], J.B. Lebert[38], H. Lee[100], S. Lee[57], I. Legrand[44], G. Legras[123], A.M. Lejeune[34], T.M. Lelek[2], I. León Monzón[105], M.M. Lesch[92], P. Lévai[45], M. Li[6], P. Li[10], X. Li[10], B.E. Liang-Gilman[18], J. Lien[118], R. Lietava[97], I. Likmeta[112], B. Lim[55], H. Lim[16], S.H. Lim[16], Y.N. Lima[106], S. Lin[10], V. Lindenstruth[38], C. Lippmann[94], D. Liskova[102], D.H. Liu[6], J. Liu[115], Y. Liu[6], G.S.S. Liveraro[107], I.M. Lofnes[20,37], C. Loizides[20], S. Lokos[103], J. Lömker[58], X. Lopez[124], E. López Torres[7], C. Lotteau[125], P. Lu[116], W. Lu[6], Z. Lu[10], O. Lubynets[94], G.A. Lucia[29], F.V. Lugo[66], J. Luo[39], G. Luparello[56], Y.G. Ma[39], V. Machacek[80], M. Mager[32], M. Mahlein[92], A. Maire[126], E. Majerz[2], M.V. Makariev[35], G. Malfattore[50], N. Malik[15], N.M. Malik[88], D. Mallick[128], N. Mallick[113], G. Mandaglio[30,52], S. Mandal[77], S.K. Mandal[76], A. Manea[62], R. Manhart[92], A.K. Manna[47], F. Manso[124], G. Mantzaridis[92], V. Manzari[49], Y. Mao[6], R.W. Marcjan[2], G.V. Margagliotti[23], A. Margotti[50], A. Marín[94], C. Markert[104], P. Martinengo[32], M.I. Martínez[43], M.P.P. Martins[32,106], S. Masciocchi[94], M. Masera[24], A. Masoni[51], L. Massacrier[128], O. Massen[58], A. Mastroserio[49,129], L. Mattei[24,124], S. Mattiazzo[27], A. Matyja[103], J.L. Mayo[104], F. Mazzaschi[32], M. Mazzilli[31], Y. Melikyan[42], M. Melo[106], A. Menchaca-Rocha[66], J.E.M. Mendez[64], E. Meninno[73], M.W. Menzel[32,91], M. Meres[13], L. Micheletti[55], D. Mihai[109], D.L. Mihaylov[92], A.U. Mikalsen[20], K. Mikhaylov[139], L. Millot[70], N. Minafra[114,g], D. Miśkowiec[94], A. Modak[56], B. Mohanty[77], M. Mohisin Khan[15,h], M.A. Molander[42], M.M. Mondal[77], S. Monira[133], D.A. Moreira De Godoy[123], A. Morsch[32], C. Moscatelli[23], T. Mrnjavac[32], S. Mrozinski[63], V. Muccifora[48], S. Muhuri[132], A. Mulliri[22], M.G. Munhoz[106], R.H. Munzer[63], L. Musa[32], J. Musinsky[59], J.W. Myrcha[133], B. Naik[120], A.I. Nambrath[18], B.K. Nandi[46], R. Nania[50], E. Nappi[49], A.F. Nassirpour[17], V. Nastase[109], A. Nath[91], N.F. Nathanson[80], A. Neagu[19], L. Nellen[64], R. Nepeivoda[72], S. Nese[19], N. Nicassio[31], B.S. Nielsen[80], E.G. Nielsen[80], F. Noferini[50], S. Noh[12], P. Nomokonov[139], J. Norman[115], N. Novitzky[84], J. Nystrand[20], M.R. Ockleton[115], M. Ogino[74], J. Oh[16], S. Oh[17], A. Ohlson[72], M. Oida[89], L.A.D. Oliveira[107], C. Oppedisano[55], A. Ortiz Velasquez[64], H. Osanai[74], J. Otwinowski[103], M. Oya[89], K. Oyama[74], S. Padhan[46,131], D. Pagano[54,131], V. Pagliarino[55], G. Paić[64], A. Palasciano[49,93], I. Panasenko[72], P. Panigrahi[46], C. Pantouvakis[27], H. Park[122], J. Park[122], S. Park[100], T.Y. Park[137], J.E. Parkkila[133], P.B. Pati[80], Y. Patley[46], R.N. Patra[49], J. Patter[47], B. Paul[132], F. Pazdic[97], H. Pei[6], T. Peitzmann[58], X. Peng[11,53], S. Perciballi[24], G.M. Perez[7], M. Petrovici[44], S. Piano[56], M. Pikna[13], P. Pillot[99], O. Pinazza[32,50], C. Pinto[32], S. Pisano[48], A. Plachta[133], M. Planinic[86], D.K. Plociennik[2], M. Płoskoń[71], S. Politano[32], N. Poljak[86], A. Pop[44], S. Porteboeuf-Houssais[124], J.S. Potgieter[110], I.Y. Pozos[43], K.K. Pradhan[47], S. Prasad[45,47], S.K. Prasad[4], R. Preghenella[50], F. Prino[55], C.A. Pruneau[134], M. Puccio[32], S. Pucillo[28], S. Pulawski[117], L. Quaglia[24], A.M.K. Radhakrishnan[47], S. Ragoni[14], A. Rai[135], A. Rakotozafindrabe[127], N. Ramasubramanian[125], L. Ramello[55,130], C.O. Ramírez-Álvarez[43], M. Rasa[26], S.S. Räsänen[42], R. Rath[94], M.P. Rauch[20], I. Ravasenga[32], M. Razza[25], K.F. Read[84,119],



JHEP07(2026)051

C. Reckziegel[108], A.R. Redelbach[38], K. Redlich[76,i], H.D. Regules-Medel[43], A. Rehman[20], F. Reidt[32], H.A. Reme-Ness[37], K. Reygers[91], M. Richter[20], A.A. Riedel[92], W. Riegler[32], A.G. Riffero[24], M. Rignanese[27], C. Ripoli[28], C. Ristea[62], M.V. Rodriguez[32], M. Rodríguez Cahuantzi[43], K. Røed[19], E. Rogochaya[139], D. Rohr[32], D. Röhrich[20], S. Rojas Torres[34], P.S. Rokita[133], G. Romanenko[25], F. Ronchetti[32], D. Rosales Herrera[43], K. Roslon[133], A. Rossi[53], A. Roy[47], A. Roy[118], S. Roy[46], N. Rubini[50], O. Rubza[15], J.A. Rudolph[81], D. Ruggiano[133], R. Rui[23], P.G. Russek[2], A. Rustamov[78], A. Rybicki[103], L.C.V. Ryder[114], G. Ryu[69], J. Ryu[16], W. Rzesa[92], B. Sabiu[50], R. Sadek[71], S. Sadhu[41], A. Saha[31], S. Saha[46,77], B. Sahoo[47], R. Sahoo[47], D. Sahu[64], P.K. Sahu[60], J. Saini[132], S. Sakai[122], S. Sambyal[88], D. Samitz[73], I. Sanna[32], D. Sarkar[80], V. Sarritzu[22], V.M. Sarti[92], M.H.P. Sas[81], U. Savino[24], S. Sawan[77], E. Scapparone[50], J. Schambach[84], H.S. Scheid[32], C. Schiaua[44], R. Schicker[91], F. Schlepper[32,91], A. Schmah[94], C. Schmidt[94], M. Schmidt[90], J. Schoengarth[63], R. Schotter[73], A. Schröter[38], J. Schukraft[32], K. Schweda[94], G. Scioli[25], E. Scomparin[55], J.E. Seger[14], D. Sekihata[121], M. Selina[81], I. Selyuzhenkov[94], S. Senyukov[126], J.J. Seo[91], L. Serkin[64,j], L. Šerkšnytė[32], A. Sevcenco[62], T.J. Shaba[67], A. Shabetai[99], R. Shahoyan[32], B. Sharma[88], D. Sharma[46], H. Sharma[53], M. Sharma[88], S. Sharma[88], T. Sharma[40], U. Sharma[88], O. Sheibani[134], K. Shigaki[89], M. Shimomura[75], Q. Shou[39], S. Siddhanta[51], T. Siemiarczuk[76], T.F. Silva[106], W.D. Silva[106], D. Silvermyr[72], T. Simantathammakul[101], R. Simeonov[35], B. Singh[46], B. Singh[88], B. Singh[92], K. Singh[47], R. Singh[77], R. Singh[53], S. Singh[15], T. Sinha[96], B. Sitar[13], M. Sitta[55,130], T.B. Skaali[19], G. Skorodumovs[91], N. Smirnov[135], K.L. Smith[16], R.J.M. Snellings[58], E.H. Solheim[19], S. Solokhin[81], C. Sonnabend[32,94], J.M. Sonneveld[81], F. Soramel[27], A.B. Soto-Hernandez[85], R. Spijkers[81], C. Sporleder[113], I. Sputowska[103], J. Staa[72], J. Stachel[91], L.L. Stahl[106], I. Stan[62], A.G. Stejskal[114], T. Stellhorn[123], S.F. Stiefelmaier[91], D. Stocco[99], I. Storehaug[19], N.J. Strangmann[63], P. Stratmann[123], S. Strazzi[25], A. Sturniolo[30,52,115], Y. Su[6], A.A.P. Suaide[106], C. Suire[128], A. Suiu[109], M. Suljic[32], V. Sumberia[88], S. Sumowidagdo[79], P. Sun[10], N.B. Sundstrom[58], L.H. Tabares[7], A. Tabikh[70], S.F. Taghavi[92], J. Takahashi[107], M.A. Talamantes Johnson[43], G.J. Tambave[77], Z. Tang[116], J. Tanwar[87], J.D. Tapia Takaki[114], N. Tapus[109], L.A. Tarasovicova[36], M.G. Tarzila[44], A. Tauro[32], A. Tavira García[104,128], G. Tejeda Muñoz[43], L. Terlizzi[24], C. Terrevoli[49], D. Thakur[55], S. Thakur[4], M. Thogersen[19], D. Thomas[104], A.M. Tiekoetter[123], N. Tiltmann[32,123], A.R. Timmins[112], A. Toia[63], R. Tokumoto[89], S. Tomassini[25], K. Tomohiro[89], Q. Tong[6], V.V. Torres[99], A. Trifiró[30,52], T. Triloki[93], A.S. Triolo[32], S. Tripathy[32], T. Tripathy[124], S. Trogolo[24], V. Trubnikov[3], W.H. Trzaska[113], T.P. Trzcinski[133], C. Tsolanta[19], R. Tu[39], R. Turrisi[53], T.S. Tveter[19], K. Ullaland[20], B. Ulukutlu[92], S. Upadhyaya[103], A. Uras[125], M. Urioni[23], G.L. Usai[22], M. Vaid[88], M. Vala[36], N. Valle[54], L.V.R. van Doremalen[58], M. van Leeuwen[81], R.J.G. van Weelden[81], D. Varga[45], Z. Varga[135], P. Vargas Torres[64], O. Vázquez Doce[48], O. Vazquez Rueda[112], G. Vecil[23,b], P. Veen[127], E. Vercellin[24], R. Verma[46], R. Vértesi[45], M. Verweij[58], L. Vickovic[33], Z. Vilakazi[120], A. Villani[23], C.J.D. Villiers[67], T. Virgili[28], M.M.O. Virta[42,80], A. Vodopyanov[139], M.A. Völkl[97], S.A. Voloshin[134], G. Volpe[31], B. von Haller[32], I. Vorobyev[32], J. Vrláková[36], J. Wan[39], C. Wang[39], D. Wang[39], Y. Wang[116], Y. Wang[39], Y. Wang[6], Z. Wang[39], F. Weiglhofer[32], S.C. Wenzel[32], J.P. Wessels[123], P.K. Wiacek[2], J. Wiechula[63], J. Wikne[19], G. Wilk[76], J. Wilkinson[94], G.A. Willems[123], N. Wilson[115], B. Windelband[91], J. Witte[91], M. Wojnar[2], C.I. Worek[2], J.R. Wright[104], C.-T. Wu[6,27], W. Wu[39,92], Y. Wu[116], K. Xiong[39], Z. Xiong[116], L. Xu[6,125], R. Xu[6], Z. Xue[71], A. Yadav[41], A.K. Yadav[132], Y. Yamaguchi[89], S. Yang[57], S. Yang[20], S. Yano[89], Z. Ye[71], E.R. Yeats[18], J. Yi[6], R. Yin[39], Z. Yin[6], I.-K. Yoo[16], J.H. Yoon[57], H. Yu[12], S. Yuan[20], A. Yuncu[91], V. Zaccolo[23], C. Zampolli[32], F. Zanone[91], N. Zardoshti[32], P. Závada[61], B. Zhang[91], C. Zhang[127], M. Zhang[6,124], M. Zhang[6,27], S. Zhang[39], X. Zhang[6], Y. Zhang[116], Y. Zhang[116], Z. Zhang[6], D. Zhou[6], Y. Zhou[80], Z. Zhou[39], J. Zhu[39], S. Zhu[94,116], Y. Zhu[6], A. Zingaretti[27], S.C. Zugravel[55], N. Zurlo[54,131]

[1] *A.I. Alikhanyan National Science Laboratory (Yerevan Physics Institute) Foundation, Yerevan, Armenia*
[2] *AGH University of Krakow, Cracow, Poland*
[3] *Bogolyubov Institute for Theoretical Physics, National Academy of Sciences of Ukraine, Kyiv, Ukraine*
[4] *Bose Institute, Department of Physics and Centre for Astroparticle Physics and Space Science (CAPSS), Kolkata, India*
[5] *California Polytechnic State University, San Luis Obispo, California, U.S.A.*
[6] *Central China Normal University, Wuhan, China*
[7] *Centro de Aplicaciones Tecnológicas y Desarrollo Nuclear (CEADEN), Havana, Cuba*
[8] *Centro de Investigación y de Estudios Avanzados (CINVESTAV), Mexico City and Mérida, Mexico*
[9] *Chicago State University, Chicago, Illinois, U.S.A.*
[10] *China Nuclear Data Center, China Institute of Atomic Energy, Beijing, China*
[11] *China University of Geosciences, Wuhan, China*
[12] *Chungbuk National University, Cheongju, Republic of Korea*
[13] *Comenius University Bratislava, Faculty of Mathematics, Physics and Informatics, Bratislava, Slovak Republic*
[14] *Creighton University, Omaha, Nebraska, U.S.A.*
[15] *Department of Physics, Aligarh Muslim University, Aligarh, India*
[16] *Department of Physics, Pusan National University, Pusan, Republic of Korea*
[17] *Department of Physics, Sejong University, Seoul, Republic of Korea*
[18] *Department of Physics, University of California, Berkeley, California, U.S.A.*
[19] *Department of Physics, University of Oslo, Oslo, Norway*
[20] *Department of Physics and Technology, University of Bergen, Bergen, Norway*
[21] *Dipartimento di Fisica, Università di Pavia, Pavia, Italy*
[22] *Dipartimento di Fisica dell'Università and Sezione INFN, Cagliari, Italy*
[23] *Dipartimento di Fisica dell'Università and Sezione INFN, Trieste, Italy*
[24] *Dipartimento di Fisica dell'Università and Sezione INFN, Turin, Italy*
[25] *Dipartimento di Fisica e Astronomia dell'Università and Sezione INFN, Bologna, Italy*
[26] *Dipartimento di Fisica e Astronomia dell'Università and Sezione INFN, Catania, Italy*
[27] *Dipartimento di Fisica e Astronomia dell'Università and Sezione INFN, Padova, Italy*
[28] *Dipartimento di Fisica 'E.R. Caianiello' dell'Università and Gruppo Collegato INFN, Salerno, Italy*
[29] *Dipartimento DISAT del Politecnico and Sezione INFN, Turin, Italy*
[30] *Dipartimento di Scienze MIFT, Università di Messina, Messina, Italy*
[31] *Dipartimento Interateneo di Fisica 'M. Merlin' and Sezione INFN, Bari, Italy*
[32] *European Organization for Nuclear Research (CERN), Geneva, Switzerland*
[33] *Faculty of Electrical Engineering, Mechanical Engineering and Naval Architecture, University of Split, Split, Croatia*
[34] *Faculty of Nuclear Sciences and Physical Engineering, Czech Technical University in Prague, Prague, Czech Republic*
[35] *Faculty of Physics, Sofia University, Sofia, Bulgaria*
[36] *Faculty of Science, P.J. Šafárik University, Košice, Slovak Republic*
[37] *Faculty of Technology, Environmental and Social Sciences, Bergen, Norway*

[38] *Frankfurt Institute for Advanced Studies, Johann Wolfgang Goethe-Universität Frankfurt, Frankfurt, Germany*
[39] *Fudan University, Shanghai, China*
[40] *Gauhati University, Department of Physics, Guwahati, India*
[41] *Helmholtz-Institut für Strahlen- und Kernphysik, Rheinische Friedrich-Wilhelms-Universität Bonn, Bonn, Germany*
[42] *Helsinki Institute of Physics (HIP), Helsinki, Finland*
[43] *High Energy Physics Group, Universidad Autónoma de Puebla, Puebla, Mexico*
[44] *Horia Hulubei National Institute of Physics and Nuclear Engineering, Bucharest, Romania*
[45] *HUN-REN Wigner Research Centre for Physics, Budapest, Hungary*
[46] *Indian Institute of Technology Bombay (IIT), Mumbai, India*
[47] *Indian Institute of Technology Indore, Indore, India*
[48] *INFN, Laboratori Nazionali di Frascati, Frascati, Italy*
[49] *INFN, Sezione di Bari, Bari, Italy*
[50] *INFN, Sezione di Bologna, Bologna, Italy*
[51] *INFN, Sezione di Cagliari, Cagliari, Italy*
[52] *INFN, Sezione di Catania, Catania, Italy*
[53] *INFN, Sezione di Padova, Padova, Italy*
[54] *INFN, Sezione di Pavia, Pavia, Italy*
[55] *INFN, Sezione di Torino, Turin, Italy*
[56] *INFN, Sezione di Trieste, Trieste, Italy*
[57] *Inha University, Incheon, Republic of Korea*
[58] *Institute for Gravitational and Subatomic Physics (GRASP), Utrecht University/Nikhef, Utrecht, Netherlands*
[59] *Institute of Experimental Physics, Slovak Academy of Sciences, Košice, Slovak Republic*
[60] *Institute of Physics, Homi Bhabha National Institute, Bhubaneswar, India*
[61] *Institute of Physics of the Czech Academy of Sciences, Prague, Czech Republic*
[62] *Institute of Space Science (ISS), Bucharest, Romania*
[63] *Institut für Kernphysik, Johann Wolfgang Goethe-Universität Frankfurt, Frankfurt, Germany*
[64] *Instituto de Ciencias Nucleares, Universidad Nacional Autónoma de México, Mexico City, Mexico*
[65] *Instituto de Física, Universidade Federal do Rio Grande do Sul (UFRGS), Porto Alegre, Brazil*
[66] *Instituto de Física, Universidad Nacional Autónoma de México, Mexico City, Mexico*
[67] *iThemba LABS, National Research Foundation, Somerset West, South Africa*
[68] *Jeonbuk National University, Jeonju, Republic of Korea*
[69] *Korea Institute of Science and Technology Information, Daejeon, Republic of Korea*
[70] *Laboratoire de Physique Subatomique et de Cosmologie, Université Grenoble-Alpes, CNRS-IN2P3, Grenoble, France*
[71] *Lawrence Berkeley National Laboratory, Berkeley, California, U.S.A.*
[72] *Lund University Department of Physics, Division of Particle Physics, Lund, Sweden*
[73] *Marietta Blau Institute, Vienna, Austria*
[74] *Nagasaki Institute of Applied Science, Nagasaki, Japan*
[75] *Nara Women's University (NWU), Nara, Japan*
[76] *National Centre for Nuclear Research, Warsaw, Poland*
[77] *National Institute of Science Education and Research, Homi Bhabha National Institute, Jatni, India*
[78] *National Nuclear Research Center, Baku, Azerbaijan*
[79] *National Research and Innovation Agency – BRIN, Jakarta, Indonesia*
[80] *Niels Bohr Institute, University of Copenhagen, Copenhagen, Denmark*
[81] *Nikhef, National institute for subatomic physics, Amsterdam, Netherlands*
[82] *Nuclear Physics Group, STFC Daresbury Laboratory, Daresbury, U.K.*
[83] *Nuclear Physics Institute of the Czech Academy of Sciences, Husinec-Řež, Czech Republic*
[84] *Oak Ridge National Laboratory, Oak Ridge, Tennessee, U.S.A.*
[85] *Ohio State University, Columbus, Ohio, U.S.A.*
[86] *Physics department, Faculty of science, University of Zagreb, Zagreb, Croatia*



JHEP07(2026)051

[87] *Physics Department, Panjab University, Chandigarh, India*
[88] *Physics Department, University of Jammu, Jammu, India*
[89] *Physics Program and International Institute for Sustainability with Knotted Chiral Meta Matter (WPI-SKCM$^2$), Hiroshima University, Hiroshima, Japan*
[90] *Physikalisches Institut, Eberhard-Karls-Universität Tübingen, Tübingen, Germany*
[91] *Physikalisches Institut, Ruprecht-Karls-Universität Heidelberg, Heidelberg, Germany*
[92] *Physik Department, Technische Universität München, Munich, Germany*
[93] *Politecnico di Bari, Bari, Italy*
[94] *Research Division and ExtreMe Matter Institute EMMI, GSI Helmholtzzentrum für Schwerionenforschung GmbH, Darmstadt, Germany*
[95] *Saga University, Saga, Japan*
[96] *Saha Institute of Nuclear Physics, Homi Bhabha National Institute, Kolkata, India*
[97] *School of Physics and Astronomy, University of Birmingham, Birmingham, U.K.*
[98] *Sección Física, Departamento de Ciencias, Pontificia Universidad Católica del Perú, Lima, Peru*
[99] *SUBATECH, IMT Atlantique, Nantes Université, CNRS-IN2P3, Nantes, France*
[100] *Sungkyunkwan University, Suwon City, Republic of Korea*
[101] *Suranaree University of Technology, Nakhon Ratchasima, Thailand*
[102] *Technical University of Košice, Košice, Slovak Republic*
[103] *The Henryk Niewodniczanski Institute of Nuclear Physics, Polish Academy of Sciences, Cracow, Poland*
[104] *The University of Texas at Austin, Austin, Texas, U.S.A.*
[105] *Universidad Autónoma de Sinaloa, Culiacán, Mexico*
[106] *Universidade de São Paulo (USP), São Paulo, Brazil*
[107] *Universidade Estadual de Campinas (UNICAMP), Campinas, Brazil*
[108] *Universidade Federal do ABC, Santo Andre, Brazil*
[109] *Universitatea Nationala de Stiinta si Tehnologie Politehnica Bucuresti, Bucharest, Romania*
[110] *University of Cape Town, Cape Town, South Africa*
[111] *University of Derby, Derby, U.K.*
[112] *University of Houston, Houston, Texas, U.S.A.*
[113] *University of Jyväskylä, Jyväskylä, Finland*
[114] *University of Kansas, Lawrence, Kansas, U.S.A.*
[115] *University of Liverpool, Liverpool, U.K.*
[116] *University of Science and Technology of China, Hefei, China*
[117] *University of Silesia in Katowice, Katowice, Poland*
[118] *University of South-Eastern Norway, Kongsberg, Norway*
[119] *University of Tennessee, Knoxville, Tennessee, U.S.A.*
[120] *University of the Witwatersrand, Johannesburg, South Africa*
[121] *University of Tokyo, Tokyo, Japan*
[122] *University of Tsukuba, Tsukuba, Japan*
[123] *Universität Münster, Institut für Kernphysik, Münster, Germany*
[124] *Université Clermont Auvergne, CNRS/IN2P3, LPC, Clermont-Ferrand, France*
[125] *Université de Lyon, CNRS/IN2P3, Institut de Physique des 2 Infinis de Lyon, Lyon, France*
[126] *Université de Strasbourg, CNRS, IPHC UMR 7178, F-67000 Strasbourg, France, Strasbourg, France*
[127] *Université Paris-Saclay, Centre d'Etudes de Saclay (CEA), IRFU, Départment de Physique Nucléaire (DPhN), Saclay, France*
[128] *Université Paris-Saclay, CNRS/IN2P3, IJCLab, Orsay, France*
[129] *Università degli Studi di Foggia, Foggia, Italy*
[130] *Università del Piemonte Orientale, Vercelli, Italy*
[131] *Università di Brescia, Brescia, Italy*
[132] *Variable Energy Cyclotron Centre, Homi Bhabha National Institute, Kolkata, India*
[133] *Warsaw University of Technology, Warsaw, Poland*
[134] *Wayne State University, Detroit, Michigan, U.S.A.*
[135] *Yale University, New Haven, Connecticut, U.S.A.*
[136] *Yildiz Technical University, Istanbul, Turkey*

JHEP07(2026)051

[137] *Yonsei University, Seoul, Republic of Korea*
[138] *Affiliated with an institute formerly covered by a cooperation agreement with CERN*
[139] *Affiliated with an international laboratory covered by a cooperation agreement with CERN*

[a] *Also at INFN Trieste, Trieste, Italy*
[b] *Also at Fondazione Bruno Kessler (FBK), Trento, Italy*
[c] *Also at Max-Planck-Institut fur Physik, Munich, Germany*
[d] *Also at Czech Technical University in Prague, Prague, Czech Republic*
[e] *Also at Instituto de Fisica da Universidade de Sao Paulo*
[f] *Also at Dipartimento DET del Politecnico di Torino, Turin, Italy*
[g] *Also at University College of Dublin, Dublin, Ireland*
[h] *Also at Department of Applied Physics, Aligarh Muslim University, Aligarh, India*
[i] *Also at Institute of Theoretical Physics, University of Wroclaw, Wroclaw, Poland*
[j] *Also at Facultad de Ciencias, Universidad Nacional Autónoma de México, Mexico City, Mexico*
[†] *Deceased*

JHEP07(2026)051